# Spontaneous emission in a planar Fabry-Pérot microcavity

S. M. Dutra and P. L. Knight
*Optics Section, The Blackett Laboratory, Imperial College, Prince Consort Road, London SW7 2BZ, United Kingdom*
(Received 19 September 1995)

We study the spontaneous-emission of a single atom located between two parallel infinite plates where one of the plates is partially reflective and the plate separation is of the order of the wavelength of the atomic transition. We pay particular attention to the nature of the field modes in such a finite finesse cavity, including the full three-dimensional nature of the field. We then compute the decay rate of an excited atom placed inside such a cavity. The angular distributions of the spontaneous-emission and of the cavity field vacuum fluctuation variances are investigated. Finally, we examine the output field from an atom inside a finite finesse microcavity. We show that the radiation transmitted outside such microcavity forms a nondiffracting Bessel beam.

PACS number(s): 42.50.Dv, 42.50.Lc, 42.55.−f

## I. INTRODUCTION

The microwave regime has many practical advantages over the optical regime for the realization of cavity QED effects [1,2]. Single-mode high-$Q$ microwave cavities are easier to engineer than their optical counterparts: single-mode microwave cavities have dimensions of the order of millimeters while single-mode optical cavities must be as small as a few micrometers. The optical regime requires high-quality factors and often relies on mode degeneracies. In addition, electric-dipole moments associated with optical transitions are much smaller than those associated with microwave transitions of Rydberg atoms. Such high-quality factors are difficult to reach, given that ordinary metal mirrors tend to be rather lossy in the optical regime.

Despite all these difficulties, cavity QED in the optical regime has attracted a great deal of interest [3]. Inhibition of spontaneous-emission was demonstrated in the optical regime in a single-mode cavity [4,5], with mirror separation of the order of an optical wavelength (a few thousands of angstroms), and in a confocal resonator, with mirror separation of the order of 1 mm, exploiting the large mode degeneracy to create substantial cavity modified fields [6]. More recently, An *et al.* [7] employed a confocal resonator, with mirrors of extremely high reflectivity yielding a $Q$ of about $8\times10^5$, to operate the first one-atom laser.

It has been proposed that the concept of energy band gaps could be extended to photons [8,9]. Electronic energy band gaps arise for electrons in solids where the atoms are arranged periodically in space [10]. The similarity [9,11–13] between Schrödinger's equation and Helmholtz's equation suggests that a periodic dielectric would give rise to gaps in the electromagnetic mode density, i.e., to the absence of modes for certain frequency intervals. Now, if a defect is introduced in the periodic dielectric, a single mode can be created within the gap, just as a defect in a crystal can generate a discrete energy state within an energy band gap [10]. This would then constitute a single-mode high-$Q$ cavity that could be engineered to operate in the optical regime. In order to have a true photonic band gap, the dielectric must be periodic in all three dimensions [13,12]. Nonetheless, periodicity in one dimension only already gives rise to some interesting effects. A mirror can be built by stacking alternating layers of two different kinds of material, one with very high dielectric constant and another with very low dielectric constant [14,15]. The overall reflectivity of the stack can be made very high due to interferences between the partial reflections on each layer [16]. For this reason such a mirror is called a distributed Bragg reflector, or DBR for short.

DBR mirrors found an important application in the development of vertical cavity semiconductor lasers [17], where the vertical configuration reduces the length of gain media crossed by light on each round-trip in the cavity from a few hundred micrometers to only about 1 $\mu$m [18]. In order to make such a device lase, the number of round-trips has to be increased. A conventional semiconductor laser relies on the 30% reflectivity given by the interface of air with the cleaved edges of the semiconductor block to provide the few round-trips it needs to lase [19]. Recent developments in molecular-beam epitaxy and ion implantation have now enabled the etching of distributed Bragg reflectors in a scale of micrometers [17]. Such DBR mirrors have been used to build planar Fabry-Pérot microcavities, which allowed the operation of vertical cavity semiconductor microlasers with threshold currents much lower than in conventional semiconductor lasers [14,15,20]. Because DBR microcavities have dimensions of the order of the lasing wavelength, they are expected to show some cavity QED effects such as modified spontaneous-emission rates that would give microlasers unconventional properties, e.g., thresholdless lasing [21,22] and faster response to modulation than conventional semiconductor lasers [23]. Distributed Bragg reflectors are far from being perfect mirrors. Their reflectivity decreases appreciably for oblique incidences [24]. However, they do not, presumably, represent the ultimate limit of technology. We have retained in our model, described in Sec. II, one key feature of semiconductor microlasers, their planar Fabry-Pérot configuration.

The question we address here is the following: what kind of cavity QED effects, arising from the planar geometry alone, can be expected in a planar Fabry-Pérot microcavity as we vary the finesse? The planar Fabry-Pérot microcavity we study in this paper is an open cavity where the atom-field system is always in the weak-coupling regime. Instead of calculating the modes of the cavity as an isolated system and

 

then introducing the interaction with the outside by adding to the master equation a Liouvillian term describing cavity losses [25], we calculate in Sec. III the modes of the whole system: cavity and outside world. In the weak-coupling regime, a cavity cannot change the irreversible nature of spontaneous emission in free space, but it can modify the spontaneous-emission exponential decay rate [26]. In Sec. IV we study these modifications and examine their dependence on the finesse of the cavity. In Sec. V we examine the effect of the cavity on vacuum fluctuations. We will see that such a planar cavity can not only change the global spontaneous-emission rate but also make emission more directional. Then, in Sec. VI we investigate the consequences of this increased directionality on the radiation that escapes from the cavity. We calculate the field outside the cavity due to the spontaneous-emission of a single atom inside and we find that it is the field of a nondiffracting ''Bessel beam'' [27]. Finally, we summarize our results in Sec. VII. Our preliminary results were summarized earlier [28].

## II. THE CAVITY MODEL

We construct the simplest possible model of a planar Fabry-Pérot retaining the following features: the transparency of even the best mirrors that lets some of the radiation escape to the outside and the open character of such a cavity whose modes can never become completely discrete. A planar Fabry-Pérot has no lateral mirrors. As a consequence, even in the case where the plates are perfect reflectors, only the component of the wave vector normal to the plates can assume discrete values; all other components remaining continuous parameters. The second feature requires the adoption of a fully three-dimensional model. The first feature implies that the cavity is not an isolated system. In this paper we study not only the radiation in the cavity but also that which is transmitted outside. In order to be able to do so, we include the mirror transmissivity in a direct and explicit way in our model and abandon the usual separation between cavity modes and external modes. Such an approach has been adopted by a number of authors [29–38]. An added bonus of this approach is that it is not limited to low transmissivity [39,40].

Having stated what we want to include in the model, we can now exclude everything else that might complicate our analysis. We will assume that the mirrors are infinitesimally thin having no internal structure and no absorption. The inclusion in the model of the material medium of the mirror and absorption would make the quantization of the electromagnetic field much harder [41–45]. In fact, we will think of these mirrors as mere boundary conditions. We will also assume that the transverse dimensions are much larger than the plate separation so that we can approximate finite mirrors by mirrors extending all the way to infinity. Finally, there are two further simplifications: we will assume that radiation can only escape through one of the mirrors, the other one being a perfect reflector, and that there is no material medium either in the cavity or outside. Our idealized Fabry-Pérot is shown in Fig. 1. The mirrors in our model are mathematical planes, which have no thickness and extend all the way to infinity. The perfect mirror can be simulated by a plane of infinite conductivity. The semitransparent mirror, however, poses a problem. In electromagnetic theory there are two kinds of materials that can be semitransparent: partial conductors and dielectrics. We do not wish to consider the former because they exhibit absorption. The latter will not absorb if the frequency dependence of the dielectric constant can be neglected, i.e., if they can be treated as nondispersive dielectrics [46]. Any dielectric layer, however, will become completely transparent if it is made infinitesimally thin (see Sec. II B). In order to avoid this, the dielectric constant has to increase accordingly as the thickness decreases. In the following subsections we show how we can simulate our semitransparent plane by such an idealized layer of dielectric material. We begin in Sec. II A with a review of plane-wave reflection at dielectric interfaces. Then, in Sec. II B we calculate the reflection and transmission coefficients for a plane wave incident on a dielectric slab. Finally, in Sec. II C we use this result to obtain the reflectivity, transmissivity, and dielectric constant of our semitransparent plane.

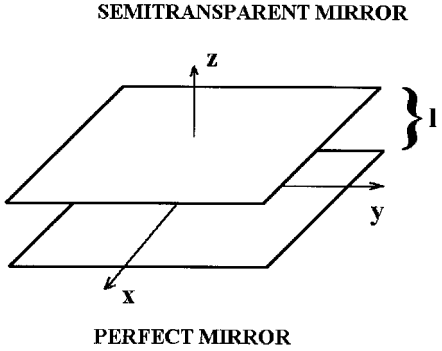


FIG. 1. Scheme of our microcavity where we have drawn the two infinite parallel planes corresponding to perfect and semitransparent mirrors separated by a distance $l$. This microcavity is an idealization of a real one where we neglect, among other things, the internal structure of the mirrors, absorption of radiation by the mirrors, and edge effects due to the finite extent of the mirrors.

### A. Dielectric interfaces

Let us consider a plane wave incident, from the vacuum, onto a dielectric medium. Unless the impedances of both media exactly match [46], there must be a reflected wave in addition to the transmitted one. The appearance of reflected and transmitted waves is an effect of the interferences between the incident wave and those emitted by each excited dipole in the dielectric medium. We will assume that they are all plane waves. The dielectric is homogeneous. This is summarized in Fig. 2.

The continuity of the component of the electric displacement perpendicular to the interface, the component of the electric field parallel to the interface, and the magnetic field (we assume that there is no magnetic medium) yield

$$E_{Ij}e^{i\boldsymbol{\kappa}_I\cdot\boldsymbol{\rho}}+E_{Rj}e^{i\boldsymbol{\kappa}_R\cdot\boldsymbol{\rho}}=E_{Tj}e^{i\boldsymbol{\kappa}_T\cdot\boldsymbol{\rho}}, \tag{2.1}$$

$$E_{Iz}e^{i\boldsymbol{\kappa}_I\cdot\boldsymbol{\rho}}+E_{Rz}e^{i\boldsymbol{\kappa}_R\cdot\boldsymbol{\rho}}=\frac{\varepsilon_d}{\varepsilon_0}E_{Tz}e^{i\boldsymbol{\kappa}_T\cdot\boldsymbol{\rho}}, \tag{2.2}$$

$$\mathbf{k}_I\wedge\mathbf{E}_Ie^{i\boldsymbol{\kappa}_I\cdot\boldsymbol{\rho}}+\mathbf{k}_R\wedge\mathbf{E}_Re^{i\boldsymbol{\kappa}_R\cdot\boldsymbol{\rho}}=\mathbf{k}_T\wedge\mathbf{E}_Te^{i\boldsymbol{\kappa}_T\cdot\boldsymbol{\rho}}, \tag{2.3}$$

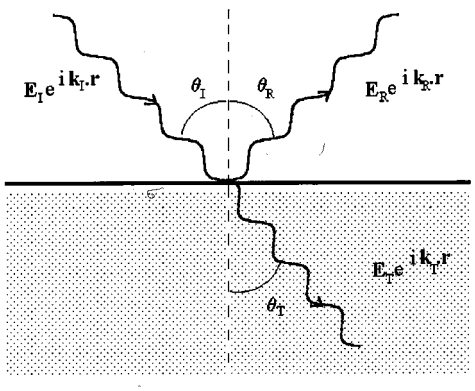


FIG. 2. Schematic representation of the reflection of a plane wave from the surface of a dielectric medium. A plane wave $\mathbf{E}_I$ with wave vector $\mathbf{k}$ propagating in the vacuum is incident at an angle $\theta_I$ on the surface of a dielectric medium of dielectric constant $\varepsilon_d$ giving rise to a reflected wave $\mathbf{E}_R$ with wave vector $\mathbf{k}$ at an angle $\theta_R$ and a transmitted wave $\mathbf{E}_T$ with wave vector $\mathbf{k}$ at an angle $\theta_T$.

where $j=x,y$ refer to components on the interface plane, $\varepsilon_d$ is the dielectric constant of the dielectric medium, $\varepsilon_0$ that of the vacuum, $I$ refers to the incident wave, $R$ to the reflected wave, and $T$ to the transmitted wave. The variable $\boldsymbol{\rho}$ gives the position on the interface plane and $\kappa_I, \kappa_R, \kappa_T$ are the projections of the corresponding wave vectors on the interface plane.

For these equations to hold at every point on the interface plane, we must have

$$\boldsymbol{\kappa}_I = \boldsymbol{\kappa}_R = \boldsymbol{\kappa}_T \equiv \boldsymbol{\kappa}. \tag{2.4}$$

From Eq. (2.4) and the wave equations for incident, reflected, and transmitted waves, we can deduce Snell's law [46]. The wave equations satisfied by these waves yield the dispersive relations between the wave number and the frequency for each medium

$$\left(\frac{\omega}{c}\right)^2 = k_I^2 = k_R^2 \tag{2.5}$$

and

$$\frac{\omega^2 \varepsilon_d}{c^2 \varepsilon_0} = k_T^2. \tag{2.6}$$

As the frequency is the same in both media, these relations imply that $n_0 k_T = n_d k_I$, where $n_0 = \sqrt{\mu_0 \varepsilon_0}$ and $n_d = \sqrt{\mu_0 \varepsilon_d}$ are the refractive indices of the vacuum and the dielectric, respectively. Using these results in (2.4), we obtain

$$\frac{\sin\theta_I}{\sin\theta_T} = n_d / n_0, \tag{2.7}$$

$$\sin\theta_R = \sin\theta_I, \tag{2.8}$$

where $\theta_I$, $\theta_R$, and $\theta_T$ are the angles of incidence, reflection, and refraction measured from the normal to the interface.

Equation (2.4) also implies that all three waves lie on the same plane. If we then use Eq. (2.5), we can write

$$\mathbf{k}_I = \boldsymbol{\kappa} + \hat{\mathbf{z}} k_{Iz}, \tag{2.9}$$

$$\mathbf{k}_R = \boldsymbol{\kappa} - \hat{\mathbf{z}} k_{Iz}, \tag{2.10}$$

$$\mathbf{k}_T = \boldsymbol{\kappa} + \hat{\mathbf{z}} k_{Tz}. \tag{2.11}$$

We now determine from the boundary conditions the amplitudes of the reflected and transmitted waves produced by the incident wave. Before doing so, we notice that the boundary condition for the magnetic field (2.3) will in general couple different components of $\mathbf{E}_I$ and $\mathbf{E}_T$. It does not couple, however, the components perpendicular to the plane of incidence with those lying on the plane of incidence. This is a consequence of the symmetry of the problem. For each wave, the electric field has to be on the plane perpendicular to its wave vector. The intersection of such three planes associated with each wave is a line perpendicular to the plane of incidence. We notice then that whenever the electric field of a wave is perpendicular to the plane of incidence, its magnetic field will lie on the plane of incidence and vice versa. So if we examine the boundary conditions again, we see that there are two sets of pairs of independent equations, one set involving only components perpendicular to the plane of incidence and another involving only components on the plane of incidence. Using the subscript $\perp$ to designate the components perpendicular to the plane of incidence and $\parallel$ to designate those on the plane of incidence, we can write these equations as

$$E_{I\perp} + E_{R\perp} = E_{T\perp},$$

$$k_I E_{I\perp} \cos\theta_I - k_R E_{R\perp} \cos\theta_R = k_T E_{T\perp} \cos\theta_T \tag{2.12}$$

and

$$E_{I\parallel} \sin\theta_I + E_{R\parallel} \sin\theta_R = (\varepsilon_d/\varepsilon_0) E_{T\parallel} \sin\theta_T,$$

$$E_{I\parallel} \cos\theta_I - E_{R\parallel} \cos\theta_R = E_{T\parallel} \cos\theta_T. \tag{2.13}$$

If we now substitute the dispersion relations (2.5) and (2.6), Snell's law (2.7), and Eq. (2.8) in Eqs. (2.12) and (2.13), we find the following expressions for the normal and parallel components of the reflected and transmitted waves:

$$E_{R\perp} = \frac{\cos\theta - \sqrt{(\varepsilon_d/\varepsilon_0) - \sin^2\theta}}{\cos\theta + \sqrt{(\varepsilon_d/\varepsilon_0) - \sin^2\theta}} E_{I\perp}, \tag{2.14}$$

$$E_{T\perp} = \frac{2\cos\theta}{\cos\theta + \sqrt{(\varepsilon_d/\varepsilon_0) - \sin^2\theta}} E_{I\parallel}, \tag{2.15}$$

$$E_{R\parallel} = \frac{(\varepsilon_d/\varepsilon_0)\cos\theta - \sqrt{(\varepsilon_d/\varepsilon_0) - \sin^2\theta}}{(\varepsilon_d/\varepsilon_0)\cos\theta + \sqrt{(\varepsilon_d/\varepsilon_0) - \sin^2\theta}} E_{I\parallel}, \tag{2.16}$$

$$E_{T\parallel} = \frac{2\sqrt{\varepsilon_d/\varepsilon_0}\cos\theta}{(\varepsilon_d/\varepsilon_0)\cos\theta + \sqrt{(\varepsilon_d/\varepsilon_0) - \sin^2\theta}} E_{I\parallel}, \tag{2.17}$$

where we have called $\theta_I$ simply $\theta$. These are Fresnel formulas for reflection and refraction of plane waves on dielectric

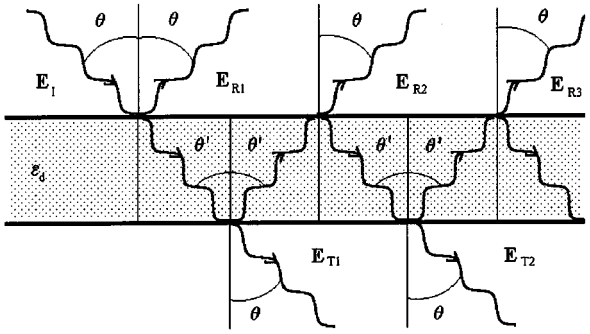


FIG. 3. Reflected and transmitted waves can be thought as resulting from the sum of all multiple reflections in the slab. The notation used in the calculations is explained in this figure.

interfaces [46], used in the next subsection to obtain expressions for the transmissivity and reflectivity of a slab of dielectric material.

### B. Thick dielectric film

Now we consider a plane wave incident on a slab of dielectric of thickness $\Delta$. The incident wave will suffer a series of reflections on each interface, being partially transmitted in each reflection as shown in Fig. 3. According to the Fresnel formulas (2.14)–(2.17), on the first interface, the amplitudes of the reflected and transmitted waves are given by

$$\begin{bmatrix} E_{R\perp} \\ E_{R\parallel} \end{bmatrix} = \begin{bmatrix} r_{1\perp}(\theta) & 0 \\ 0 & r_{1\parallel}(\theta) \end{bmatrix} \begin{bmatrix} E_{I\perp} \\ E_{I\parallel} \end{bmatrix} \tag{2.18}$$

and

$$\begin{bmatrix} E_{T\perp} \\ E_{T\parallel} \end{bmatrix} = \begin{bmatrix} t_{1\perp}(\theta) & 0 \\ 0 & t_{1\parallel}(\theta) \end{bmatrix} \begin{bmatrix} E_{I\perp} \\ E_{I\parallel} \end{bmatrix}, \tag{2.19}$$

where

$$r_{1\perp}(\theta) = \frac{\cos\theta - \sqrt{(\varepsilon_d/\varepsilon_0) - \sin^2\theta}}{\cos\theta + \sqrt{(\varepsilon_d/\varepsilon_0) - \sin^2\theta}}, \tag{2.20}$$

$$t_{1\perp}(\theta) = \frac{2\cos\theta}{\cos\theta + \sqrt{(\varepsilon_d/\varepsilon_0) - \sin^2\theta}}, \tag{2.21}$$

$$r_{1\parallel}(\theta) = \frac{(\varepsilon_d/\varepsilon_0)\cos\theta - \sqrt{(\varepsilon_d/\varepsilon_0) - \sin^2\theta}}{(\varepsilon_d/\varepsilon_0)\cos\theta + \sqrt{(\varepsilon_d/\varepsilon_0) - \sin^2\theta}}, \tag{2.22}$$

$$t_{1\parallel}(\theta) = \frac{2\sqrt{\varepsilon_d/\varepsilon_0}\cos\theta}{(\varepsilon_d/\varepsilon_0)\cos\theta + \sqrt{(\varepsilon_d/\varepsilon_0) - \sin^2\theta}}. \tag{2.23}$$

Similarly, on the second interface

$$\begin{bmatrix} E_{R\perp} \\ E_{R\parallel} \end{bmatrix} = \begin{bmatrix} r_{2\perp}(\theta') & 0 \\ 0 & r_{2\parallel}(\theta') \end{bmatrix} \begin{bmatrix} E_{I\perp} \\ E_{I\parallel} \end{bmatrix} \tag{2.24}$$

and

$$\begin{bmatrix} E_{T\perp} \\ E_{T\parallel} \end{bmatrix} = \begin{bmatrix} t_{2\perp}(\theta') & 0 \\ 0 & t_{2\parallel}(\theta') \end{bmatrix} \begin{bmatrix} E_{I\perp} \\ E_{I\parallel} \end{bmatrix}, \tag{2.25}$$

where

$$r_{2\perp}(\theta') = \frac{\cos\theta' - \sqrt{(\varepsilon_0/\varepsilon_d) - \sin^2\theta'}}{\cos\theta' + \sqrt{(\varepsilon_0/\varepsilon_d) - \sin^2\theta'}}, \tag{2.26}$$

$$t_{2\perp}(\theta') = \frac{2\cos\theta'}{\cos\theta' + \sqrt{(\varepsilon_0/\varepsilon_d) - \sin^2\theta'}}, \tag{2.27}$$

$$r_{2\parallel}(\theta') = \frac{(\varepsilon_0/\varepsilon_d)\cos\theta' - \sqrt{(\varepsilon_0/\varepsilon_d) - \sin^2\theta'}}{(\varepsilon_0/\varepsilon_d)\cos\theta' + \sqrt{(\varepsilon_0/\varepsilon_d) - \sin^2\theta'}}, \tag{2.28}$$

$$t_{2\parallel}(\theta') = \frac{2\sqrt{\varepsilon_0/\varepsilon_d}\cos\theta'}{(\varepsilon_0/\varepsilon_d)\cos\theta' + \sqrt{(\varepsilon_0/\varepsilon_d) - \sin^2\theta'}}. \tag{2.29}$$

The total transmissivity $\mathbf{T}$ and reflectivity $\mathbf{R}$ of the slab can be obtained by summing the contributions from all the multiple reflections shown in Fig. 3,

$$\begin{aligned} \mathbf{E}_T = \mathbf{T}\mathbf{E}_I &= \mathbf{E}_{T1} + \mathbf{E}_{T2} + \cdots \\ &= e^{i\delta}\mathbf{t}_2(\theta')\mathbf{t}_1(\theta)\mathbf{E}_I \\ &\quad + e^{i3\delta}\mathbf{t}_2(\theta')\mathbf{r}_2(\theta')\mathbf{r}_2(\theta')\mathbf{t}_1(\theta)\mathbf{E}_I + \cdots \\ &= e^{i\delta}\mathbf{t}_2(\theta')\left\{\sum_{n=0}^{\infty}[\mathbf{r}_2(\theta')e^{i\delta}]^{2n}\right\}\mathbf{t}_1(\theta)\mathbf{E}_I \end{aligned} \tag{2.30}$$

and

$$\begin{aligned} \mathbf{E}_R = \mathbf{R}\mathbf{E}_I &= \mathbf{E}_{R1} + \mathbf{E}_{R2} + \cdots \\ &= \mathbf{r}_1(\theta)\mathbf{E}_I + e^{i2\delta}\mathbf{t}_2(\theta')\mathbf{r}_2(\theta')\mathbf{t}_1(\theta)\mathbf{E}_I + \cdots \\ &= \left(\mathbf{r}_1(\theta) + e^{i\delta}\mathbf{t}_2(\theta')\right. \\ &\quad \left.\times\left\{\sum_{n=0}^{\infty}[\mathbf{r}_2(\theta')e^{i\delta}]^{2n+1}\right\}\mathbf{t}_1(\theta)\right)\mathbf{E}_I, \end{aligned} \tag{2.31}$$

where $\mathbf{t}_1$ is the $2\times2$ matrix on the right-hand side of Eq. (2.19), $\mathbf{t}_2$ is that on the right-hand side of (2.25), $\mathbf{r}_1,\mathbf{r}_2$ are those in (2.18) and (2.24), and the phase difference $\delta$ is given by

$$\delta = \frac{\omega}{c}\sqrt{\frac{\varepsilon_d}{\varepsilon_0}}\Delta\,\cos\theta'. \tag{2.32}$$

Performing the sums in (2.30) and (2.31) we find

$$\mathbf{T} = \begin{bmatrix} T_\perp & 0 \\ 0 & T_\parallel \end{bmatrix} \tag{2.33}$$

and

$$\mathbf{T} = \begin{bmatrix} R_\perp & 0 \\ 0 & R_\parallel \end{bmatrix}, \tag{2.34}$$

where

$$T_\perp=\frac{t_{1\perp}(\theta)t_{2\perp}(\theta')\exp(i\delta)}{1-[r_{2\perp}(\theta')\exp(i\delta)]^2}, \tag{2.35}$$

$$T_\parallel=\frac{t_{1\parallel}(\theta)t_{2\parallel}(\theta')\exp(i\delta)}{1-[r_{2\parallel}(\theta')\exp(i\delta)]^2}, \tag{2.36}$$

$$R_\perp=\frac{r_{1\perp}(\theta)+r_{2\perp}(\theta')\exp(i2\delta)}{1-[r_{2\perp}(\theta')\exp(i\delta)]^2}, \tag{2.37}$$

$$R_\parallel=\frac{r_{1\parallel}(\theta)+r_{2\parallel}(\theta')\exp(i2\delta)}{1-[r_{2\parallel}(\theta')\exp(i\delta)]^2}. \tag{2.38}$$

If we now use Snell's law (2.7) to eliminate the angle of refraction $\theta'$, we find that Eqs. (2.26)–(2.29) can be written as

$$t_{2\perp}(\theta'[\theta])=\frac{2\sqrt{(\varepsilon_d/\varepsilon_0)-\sin^2\theta}}{\cos\theta+\sqrt{(\varepsilon_d/\varepsilon_0)-\sin^2\theta}}, \tag{2.39}$$

$$r_{2\perp}(\theta'[\theta])=\frac{\sqrt{(\varepsilon_d/\varepsilon_0)-\sin^2\theta}-\cos\theta}{\cos\theta+\sqrt{(\varepsilon_d/\varepsilon_0)-\sin^2\theta}}, \tag{2.40}$$

$$r_{2\parallel}(\theta'[\theta])=\frac{\sqrt{(\varepsilon_d/\varepsilon_0)-\sin^2\theta}-(\varepsilon_d/\varepsilon_0)\cos\theta}{(\varepsilon_d/\varepsilon_0)\cos\theta+\sqrt{(\varepsilon_d/\varepsilon_0)-\sin^2\theta}}, \tag{2.41}$$

$$t_{2\parallel}(\theta'[\theta])=\frac{2\sqrt{\varepsilon_d/\varepsilon_0}\sqrt{(\varepsilon_d/\varepsilon_0)-\sin^2\theta}}{(\varepsilon_d/\varepsilon_0)\cos\theta+\sqrt{(\varepsilon_d/\varepsilon_0)-\sin^2\theta}}. \tag{2.42}$$

Comparing these equations with Eqs. (2.20)–(2.23), we find the following relations between the reflectivities and transmissivities on the second interface and those on the first interface

$$r_{2\perp}(\theta'[\theta])=-r_{1\perp}(\theta), \tag{2.43}$$

$$r_{2\parallel}(\theta'[\theta])=-r_{1\parallel}(\theta), \tag{2.44}$$

$$t_{2\perp}(\theta'[\theta])=t_{1\perp}(\theta)-2r_{1\perp}(\theta), \tag{2.45}$$

$$t_{2\parallel}(\theta'[\theta])=\frac{\varepsilon_d}{\varepsilon_0}t_{1\parallel}(\theta)-2\sqrt{\frac{\varepsilon_d}{\varepsilon_0}}r_{1\parallel}(\theta). \tag{2.46}$$

We also notice that

$$t_{1\perp}(\theta)=1+r_{1\perp}(\theta), \tag{2.47}$$

$$t_{1\parallel}(\theta)=[1+r_{1\parallel}(\theta)]\sqrt{\frac{\varepsilon_0}{\varepsilon_d}}. \tag{2.48}$$

Substituting Eqs. (2.43)–(2.48) in (2.35) to (2.38), we obtain

$$T_\perp=\frac{[1-r_{1\perp}^2(\theta)]\exp(i\delta)}{1-[r_{1\perp}(\theta)\exp(i\delta)]^2}, \tag{2.49}$$

$$T_\parallel=\frac{[1-r_{1\parallel}^2(\theta)]\exp(i\delta)}{1-[r_{1\parallel}(\theta)\exp(i\delta)]^2}, \tag{2.50}$$

$$R_\perp=\frac{[1-\exp(i2\delta)]r_{1\perp}(\theta)}{1-[r_{1\perp}(\theta)\exp(i\delta)]^2}, \tag{2.51}$$

$$R_\parallel=\frac{[1-\exp(i2\delta)]r_{1\parallel}(\theta)}{1-[r_{1\parallel}(\theta)\exp(i\delta)]^2}, \tag{2.52}$$

where

$$\delta=\frac{\omega}{c}\Delta\sqrt{\frac{\varepsilon_d}{\varepsilon_0}-\sin^2\theta}. \tag{2.53}$$

From Eqs. (2.49)–(2.53), we can see that an infinitesimally thin dielectric film, $\Delta\to 0$, of finite dielectric constant $\varepsilon_d$ will be completely transparent because

$$\lim_{\Delta\to 0} T_\perp=1, \tag{2.54}$$

$$\lim_{\Delta\to 0} T_\parallel=1, \tag{2.55}$$

$$\lim_{\Delta\to 0} R_\perp=0, \tag{2.56}$$

$$\lim_{\Delta\to 0} R_\parallel=0. \tag{2.57}$$

### C. Semitransparent plane

In this subsection we will show that we can keep the dielectric film semitransparent as it becomes infinitesimally thin, if we let the dielectric constant $\varepsilon_d$ increase proportionally so that $\varepsilon_d\Delta$ remain constant. When $\varepsilon_d$ becomes much larger than $\varepsilon_0$, the reflectivities at the first interface approach

$$r_{1\perp}(\theta)\to 2\sqrt{\frac{\varepsilon_0}{\varepsilon_d}}\cos\theta-1, \tag{2.58}$$

$$r_{1\parallel}(\theta)\to 1-2\sqrt{\frac{\varepsilon_0}{\varepsilon_d}}\sec\theta \tag{2.59}$$

and the phase difference $\delta$ approaches

$$\delta\to\frac{\omega}{c}\sqrt{\frac{\varepsilon_d}{\varepsilon_0}}\Delta. \tag{2.60}$$

Now we let $\varepsilon_d\Delta=\varepsilon_0\eta$, where $\eta$ is a constant, and we substitute Eqs. (2.58)–(2.60) in Eqs. (2.49)–(2.52) and take the limit $\Delta\to 0$, $\varepsilon_d\to\infty$. We obtain

$$\lim_{\substack{\Delta\to 0\\ \varepsilon_d\to\infty\\ \varepsilon_d\Delta=\eta\varepsilon_0}} T_\perp=\frac{2\cos\theta}{2\cos\theta-i(\omega/c)\eta}\equiv t_\perp(\theta), \tag{2.61}$$

$$\lim_{\substack{\Delta\to 0\\ \varepsilon_d\to\infty\\ \varepsilon_d\Delta=\eta\varepsilon_0}} T_\parallel=\frac{2}{2-i(\omega/c)\eta\cos\theta}\equiv t_\parallel(\theta), \tag{2.62}$$

$$\lim_{\substack{\Delta\to 0\\ \varepsilon_d\to\infty\\ \varepsilon_d\Delta=\eta\varepsilon_0}} R_\perp=\frac{i(\omega/c)\eta}{2\cos\theta-i(\omega/c)\eta}\equiv r_\perp(\theta), \qquad (2.63)$$

$$\lim_{\substack{\Delta\to 0\\ \varepsilon_d\to\infty\\ \varepsilon_d\Delta=\eta\varepsilon_0}} R_\parallel=\frac{-i(\omega/c)\eta\cos\theta}{2-i(\omega/c)\eta\cos\theta}\equiv r_\parallel(\theta). \qquad (2.64)$$

So unlike the example given at the end of Sec. II B, this is a true semitransparent plane. The parameter $\eta$ controls the transparency of the plane. From Eqs. (2.61)–(2.64), when $\eta$ vanishes the plane becomes completely transparent and when $\eta\to\infty$ the plane becomes a perfect reflector. A one-dimensional version of such a semitransparent plane was employed by a number of authors [29–31,33,36,32]. However, to our knowledge, only Ley and Loudon [36] have published expressions for the reflectivity and transmissivity of their one-dimensional version of our infinitesimally thin semitransparent mirror. Our expressions agree with theirs when we take $\theta=0$, which corresponds to normal incidence.

The reflectivities and transmissivities given in Eqs. (2.61)–(2.64) are all that we need to introduce the semitransparent plane in our cavity model. Nonetheless, let us derive an expression for the spatial dependence of the dielectric constant, because such an expression has been used as a starting point in the literature more often than Eqs. (2.61)–(2.64). In the case of the infinite slab we have studied in Sec. II B, the dielectric constant of the whole of space (we are assuming that there is nothing else in space apart from the infinite slab) is given by

$$\varepsilon(z)=[\Theta(z-l)-\Theta(z-l-\Delta)]\varepsilon_d+\varepsilon_0, \qquad (2.65)$$

where $\Theta(z)$ is the Heaviside step function, i.e., $\Theta(z)=0$ for $z<0$ and $\Theta(z)=1$ for $z>0$. We have now placed the coordinate axes so that the $z$ axis intersects the slab from $z=l$ to $z=l+\Delta$. When we take the limit that leads to the semitransparent plane, we obtain

$$\lim_{\substack{\Delta\to 0\\ \varepsilon_d\to\infty\\ \varepsilon_d\Delta=\eta\varepsilon_0}} \varepsilon(z)=\left[\lim_{\Delta\to 0}\frac{\Theta(z-l)-\Theta(z-l-\Delta)}{\Delta}\right]\eta\varepsilon_0+\varepsilon_0$$

$$=\left\{\left[\eta\frac{d\Theta(z')}{dz'}\right]_{z'=z-l}+1\right\}\varepsilon_0. \qquad (2.66)$$

As the derivative of the step function is the $\delta$ function, we can rewrite Eq. (2.66) as

$$\varepsilon(z)=[\eta\delta(z-l)+1]\varepsilon_0. \qquad (2.67)$$

## III. MODE STRUCTURE

In much of quantum optics it is assumed that the cavity modes remain those of a perfect isolated cavity, the interaction with the outside being introduced in the master equation by adding a Liouvillian loss term [25]. This approach is not advantageous when the finesse is low [39,40]. In this paper we will avoid this approach and calculate the true modes of the whole system: cavity plus outside. What is often treated as cavity modes are really the so-called Fox-Li quasi modes [47]. These quasimodes result from interferences due to successive reflections on the cavity walls that modulate the otherwise continuum set of propagating modes in free space (Fig. 4). When the finesse is high, the Fox-Li quasimodes coincide with those of a perfect lossless isolated cavity except that they have a small width, which is a function of the finite finesse [39]. For the true modes, we have also made a number of other checks of the modes we have determined, including an alternative determination of these modes directly from Maxwell's equations, verifying the field commutation relations, and recovering one-dimensional results from our three-dimensional expressions. For reasons of brevity, we include only the limit of perfect reflectivity as this has the extra benefit of helping us to understand the more interesting case of high but finite finesse.

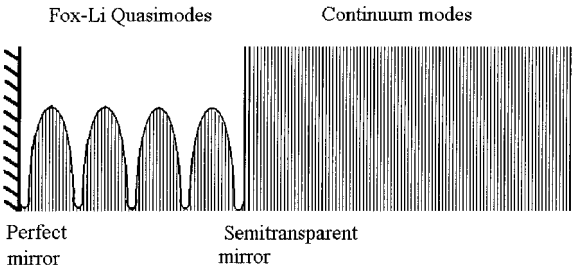


FIG. 4. Schematic representation of Fox-Li quasimodes appearing inside the cavity as modulations on the continuum of free-space modes caused by the interferences produced by multiple reflections on the cavity mirrors.

### A. Multiple-reflections approach

In the absence of a cavity, the free-space field can be written in the form of a plane-wave expansion. If we determine how the microcavity modifies each plane-wave component, we can then sum the modified components and obtain an expression for the total quantized field in the whole system. As in Sec. II, we decompose the electric field of each plane wave into two parts, a component perpendicular to the plane of incidence $\alpha=\perp$ and another component lying on the plane of incidence $\alpha=\parallel$,

$$\mathbf{E}_{I,\alpha}=\hat{\mathbf{v}}_{I,\alpha}E^0_{I,\alpha}e^{i\mathbf{k}_{I,\alpha}\cdot\mathbf{r}}, \qquad (3.1)$$

where $\hat{\mathbf{v}}_{I,\alpha}$ gives the direction of this electric-field component and $E^0_{I,\alpha}$ its amplitude. Successive reflections on the mirrors of the cavity modify these plane-wave components. We obtain the field inside the cavity due to the plane-wave component $\mathbf{E}_{I,\alpha}$ simply by adding the multiple reflections depicted in Fig. 5 [16]. In order to do so, we use the reflectivities and transmissivities of the semitransparent plane we have determined in Sec. II C. As to the perfect mirror, we assume it is a perfectly conducting plane. Because perfect conductors make the component of the electric field on their surfaces vanish, a plane wave whose electric field is perpendicular to the plane of incidence, just after being reflected off the perfect mirror, must have its electric field multiplied by

$$m_\perp=-1. \qquad (3.2)$$

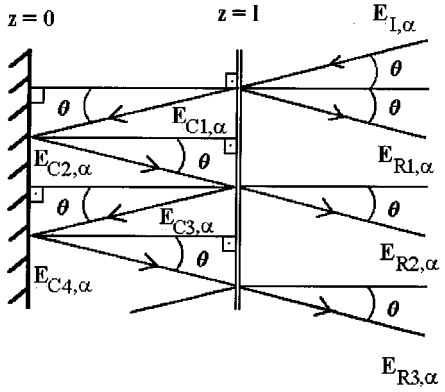


FIG. 5. Diagram of multiple reflections in the planar Fabry-Pérot cavity with the variables used in our calculations indicated in the figure.

On the other hand, when the electric field lies on the plane of incidence, it must be multiplied by

$$m_{\parallel}=1 \tag{3.3}$$

after being reflected. Using this notation, we can write

$$\begin{aligned}\mathbf{E}_{\mathrm{cav},\mathbf{k},\alpha}&=\mathbf{E}_{C1,\alpha}+\mathbf{E}_{C2,\alpha}+\cdots\\&=E^0_{I,\alpha}t_\alpha(\theta)\left(\hat{\mathbf{v}}_{I,\alpha}\left\{\sum_{n=0}^{\infty}[e^{2i\delta}m_\alpha r_\alpha(\theta)]^n\right\}e^{i\mathbf{k}_{I,\alpha}\cdot\mathbf{r}}\right.\\&\quad\left.+\hat{\mathbf{v}}_{R,\alpha}\left\{m_\alpha\sum_{n=0}^{\infty}[e^{2i\delta}m_\alpha r_\alpha(\theta)]^n\right\}e^{i\mathbf{k}_{R,\alpha}\cdot\mathbf{r}}\right)\\&=E^0_{I,\alpha}t_\alpha(\theta)\left[\frac{\hat{\mathbf{v}}_{I,\alpha}e^{i\mathbf{k}_{I,\alpha}\cdot\mathbf{r}}}{1-m_\alpha r_\alpha(\theta)e^{2i\delta}}+\frac{m_\alpha\hat{\mathbf{v}}_{R,\alpha}e^{i\mathbf{k}_{R,\alpha}\cdot\mathbf{r}}}{1-m_\alpha r_\alpha(\theta)e^{2i\delta}}\right],\end{aligned} \tag{3.4}$$

where $\hat{\mathbf{v}}_{R,\alpha}$ gives the direction of the electric field of the reflected wave and

$$\delta=\frac{\omega}{c}l\,\cos\theta \tag{3.5}$$

is the extra phase gained on each trip inside the cavity.

The field outside the cavity due to the plane-wave component $\mathbf{E}_{I,\alpha}$ is obtained by summing the plane waves on the external side of the semitransparent plane,

$$\begin{aligned}\mathbf{E}_{\mathrm{out},\mathbf{k},\alpha}&=\mathbf{E}_{I,\alpha}+\mathbf{E}_{R1,\alpha}+\mathbf{E}_{R2,\alpha}+\cdots\\&=E^0_{I,\alpha}\left\{\hat{\mathbf{v}}_{I,\alpha}e^{i\mathbf{k}_{I,\alpha}\cdot\mathbf{r}}+\hat{\mathbf{v}}_{R,\alpha}\left[r_\alpha(\theta)\right.\right.\\&\quad\left.\left.+\frac{t_\alpha(\theta)^2m_\alpha e^{2i\delta}}{1-r_\alpha(\theta)m_\alpha e^{2i\delta}}\right]e^{-i2\delta}e^{i\mathbf{k}_{R,\alpha}\cdot\mathbf{r}}\right\}\\&=E^0_{I,\alpha}\left\{\hat{\mathbf{v}}_{I,\alpha}e^{i\mathbf{k}_{I,\alpha}\cdot\mathbf{r}}\right.\\&\quad+\hat{\mathbf{v}}_{R,\alpha}\frac{r_\alpha(\theta)+[t_\alpha(\theta)^2-r_\alpha(\theta)^2]m_\alpha e^{i2\delta}}{1-r_\alpha(\theta)m_\alpha e^{i2\delta}}\\&\quad\left.\times e^{-i2\delta}e^{i\mathbf{k}_{R,\alpha}\cdot\mathbf{r}}\right\}.\end{aligned} \tag{3.6}$$

These modified plane-wave components are the modes of the system. When we substitute them for the modes of free space in the usual procedure of field quantization [35,33,36,48] we obtain the following expression for the positive-frequency component of the electric field inside and outside the microcavity (our result agrees with that of De Martini *et al.* [49], when their general result is particularized for this case):

$$\begin{aligned}\mathbf{E}^+_\alpha(\mathbf{r})=\int d^3k\{&\mathscr{E}^\alpha_\perp(\mathbf{r},\mathbf{k})\hat{\mathbf{e}}_\perp(\hat{\mathbf{k}})a_\perp(\mathbf{k})+[\mathscr{E}^\alpha_{\parallel,1}(\mathbf{r},\mathbf{k})\hat{\mathbf{e}}_{\parallel,1}(\hat{\mathbf{k}})\\&+\mathscr{E}^\alpha_{\parallel,2}(\mathbf{r},\mathbf{k})\hat{\mathbf{e}}_{\parallel,2}(\hat{\mathbf{k}})]a_\parallel(\mathbf{k})\},\end{aligned} \tag{3.7}$$

where the integration is restricted to the half space, i.e., positive $k_z$, because of the presence of the perfect mirror. We use the label $\alpha=\mathrm{cav}$ for the field inside the cavity and $\alpha=$ out for the field outside the cavity. The mode functions are given by [28]

$$\mathscr{E}^{\mathrm{cav}}_\perp(\mathbf{r},\mathbf{k})=i\mathscr{E}_{\mathrm{vac}}e^{i\boldsymbol{\kappa}\cdot\mathbf{r}}\mathscr{S}_\perp\sin(k_zz), \tag{3.8}$$

$$\mathscr{E}^{\mathrm{cav}}_{\parallel,1}(\mathbf{r},\mathbf{k})=i\mathscr{E}_{\mathrm{vac}}e^{i\boldsymbol{\kappa}\cdot\mathbf{r}}\mathscr{S}_\parallel\cos(\theta)\sin(k_zz), \tag{3.9}$$

$$\mathscr{E}^{\mathrm{cav}}_{\parallel,2}(\mathbf{r},\mathbf{k})=-\mathscr{E}_{\mathrm{vac}}e^{i\boldsymbol{\kappa}\cdot\mathbf{r}}\mathscr{S}_\parallel\sin(\theta)\cos(k_zz), \tag{3.10}$$

$$\begin{aligned}\mathscr{E}^{\mathrm{out}}_\perp(\mathbf{r},\mathbf{k})=i\mathscr{E}_{\mathrm{vac}}e^{i\boldsymbol{\kappa}\cdot\mathbf{r}}\mathscr{S}_\perp[&\sin(k_zz)-\Lambda\,\sec(\theta)\sin(\delta)\\&\times\sin(k_zz-\delta)],\end{aligned} \tag{3.11}$$

$$\begin{aligned}\mathscr{E}^{\mathrm{out}}_{\parallel,1}(\mathbf{r},\mathbf{k})=i\mathscr{E}_{\mathrm{vac}}e^{i\boldsymbol{\kappa}\cdot\mathbf{r}}\mathscr{S}_\parallel[&\sin(k_zz)-\Lambda\,\cos(\theta)\sin(\delta)\\&\times\sin(k_zz-\delta)]\cos(\theta),\end{aligned} \tag{3.12}$$

$$\begin{aligned}\mathscr{E}^{\mathrm{out}}_{\parallel,2}(\mathbf{r},\mathbf{k})=-\mathscr{E}_{\mathrm{vac}}e^{i\boldsymbol{\kappa}\cdot\mathbf{r}}\mathscr{S}_\parallel[&\cos(k_zz)-\Lambda\,\cos(\theta)\sin(\delta)\\&\times\cos(k_zz-\delta)]\sin(\theta),\end{aligned} \tag{3.13}$$

where $\boldsymbol{\kappa}$ is the projection of $\mathbf{k}$ on a plane parallel to the mirrors, $\hat{\boldsymbol{\kappa}}$ is the unit vector in the direction of $\boldsymbol{\kappa}$, $\theta$ is the angle between $\mathbf{k}$ and the $z$ axis, $\Lambda=\eta k$ is a measure of how reflective the top mirror is for a given frequency $\omega=ck$, and

$$\mathscr{E}_{\mathrm{vac}}=\sqrt{\frac{2\hbar\omega}{(2\pi)^3\varepsilon_0}} \tag{3.14}$$

is the cavity modified vacuum field strength. An extra factor of 2 as compared to the free-space vacuum field strength appears because of the perfect mirror at $z=0$ that restricts the fields to the half space. The functions $\mathscr{S}_\perp$ and $\mathscr{S}_\parallel$ describe the cavity resonances and are given by

$$\mathscr{S}_\perp=\frac{\cos(\theta)}{\cos(\theta)-\Lambda e^{i\delta}\sin(\delta)}, \tag{3.15}$$

$$\mathscr{S}_\parallel=\frac{1}{1-\Lambda e^{i\delta}\cos(\theta)\sin(\delta)}. \tag{3.16}$$

The polarization is given by the unit vectors $\hat{\mathbf{e}}_\perp(\hat{\mathbf{k}})=\hat{\mathbf{z}}\wedge\hat{\boldsymbol{\kappa}}$, $\hat{\mathbf{e}}_{\parallel,1}(\hat{\mathbf{k}})=\hat{\boldsymbol{\kappa}}$, and $\hat{\mathbf{e}}_{\parallel,2}(\hat{\mathbf{k}})=\hat{\mathbf{z}}$. The operators $a_{\mathbf{k},\alpha},a^\dagger_{\mathbf{k},\alpha}$ are the field annihilation and creation operators, respectively, for the mode $\kappa,\alpha$, with

$$[a_{\mathbf{k},\alpha},a_{\mathbf{k}',\alpha'}]=0 \tag{3.17}$$

and

$$[a_{\mathbf{k},\alpha}, a^{\dagger}_{\mathbf{k}',\alpha'}] = \delta(\mathbf{k}-\mathbf{k}')\,\delta_{\alpha,\alpha'}. \tag{3.18}$$

### B. Limit of perfect reflection

We have seen in Sec. II C that when $\eta\to\infty$, the semitransparent mirror becomes a perfect mirror with

$$\lim_{\eta\to\infty} r_{\perp} = -1, \tag{3.19}$$

$$\lim_{\eta\to\infty} t_{\perp} = 0, \tag{3.20}$$

$$\lim_{\eta\to\infty} r_{\parallel} = 1, \tag{3.21}$$

$$\lim_{\eta\to\infty} t_{\parallel} = 0. \tag{3.22}$$

In this subsection we will examine what happens to the mode structure inside the cavity in this limit.

Let us define the operators $A_{\perp}(\mathbf{k})$ and $A_{\parallel}(\mathbf{k})$ such that

$$a_{\perp}(\mathbf{k}) = \mathscr{L}^{*}_{\perp}(\mathbf{k}) A_{\perp}(\mathbf{k}), \tag{3.23}$$

$$a_{\parallel}(\mathbf{k}) = \mathscr{L}^{*}_{\parallel}(\mathbf{k}) A_{\parallel}(\mathbf{k}). \tag{3.24}$$

Then the positive-frequency component of the electric-field operator inside the cavity can be written as

$$\mathbf{E}^{+}_{\mathrm{cav}}(\mathbf{r}) = \int d^3k \{ \mathscr{U}^{\mathrm{cav}}_{\perp}(\mathbf{r},\mathbf{k}) \hat{\mathbf{e}}_{\perp}(\mathbf{k}) A_{\perp}(\mathbf{k}) + [\mathscr{U}^{\mathrm{cav}}_{\parallel,1}(\mathbf{r},\mathbf{k}) \hat{\mathbf{e}}_{\parallel,1}(\mathbf{k}) + \mathscr{U}^{\mathrm{cav}}_{\parallel,2}(\mathbf{r},\mathbf{k}) \hat{\mathbf{e}}_{\parallel,2}(\mathbf{k})] A_{\parallel}(\mathbf{k}) \}, \tag{3.25}$$

where

$$\mathscr{U}^{\mathrm{cav}}_{\perp}(\mathbf{r},\mathbf{k}) = \mathscr{E}^{\mathrm{cav}}_{\perp}(\mathbf{r},\mathbf{k}) \mathscr{L}^{*}_{\perp}(\mathbf{k}), \tag{3.26}$$

$$\mathscr{U}^{\mathrm{cav}}_{\parallel,1}(\mathbf{r},\mathbf{k}) = \mathscr{E}^{\mathrm{cav}}_{\parallel,1}(\mathbf{r},\mathbf{k}) \mathscr{L}^{*}_{\parallel}(\mathbf{k}), \tag{3.27}$$

$$\mathscr{U}^{\mathrm{cav}}_{\parallel,2}(\mathbf{r},\mathbf{k}) = \mathscr{E}^{\mathrm{cav}}_{\parallel,2}(\mathbf{r},\mathbf{k}) \mathscr{L}^{*}_{\parallel}(\mathbf{k}). \tag{3.28}$$

We notice that $\mathscr{U}^{\mathrm{cav}}_{\perp}(\mathbf{r},\mathbf{k})$ is proportional to $|\mathscr{L}_{\perp}|^2$, while both $\mathscr{U}^{\mathrm{cav}}_{\parallel,1}(\mathbf{r},\mathbf{k})$ and $\mathscr{U}^{\mathrm{cav}}_{\parallel,2}(\mathbf{r},\mathbf{k})$ are proportional to $|\mathscr{L}_{\parallel}|^2$. As we have mentioned earlier, the functions $\mathscr{L}_{\perp}(\mathbf{k})$ and $\mathscr{L}_{\parallel}(\mathbf{k})$ describe the cavity resonances. Let us investigate what happens to $|\mathscr{L}_{\perp}|^2$ and $|\mathscr{L}_{\parallel}|^2$ when the semitransparent mirror becomes a perfect reflector.

From Eq. (3.15), we obtain

$$|\mathscr{L}_{\perp}(\mathbf{k})|^2 = \frac{(1/\Lambda^2)\cos^2\theta}{[(1/\Lambda)\cos\theta - (1/2)\sin 2k_z l]^2 + \sin^4 k_z l}. \tag{3.29}$$

When $\eta\to\infty$, $\cos\theta/\Lambda$ is a very small quantity, which we denote by $\Gamma$. So Eq. (3.29) becomes

$$|\mathscr{L}_{\perp}(\mathbf{k})|^2 = \frac{\Gamma^2}{[\Gamma - (1/2)\sin 2k_z l]^2 + \sin^4 k_z l}. \tag{3.30}$$

Resonances will occur at values of $k_z$ such that

$$\sin 2k_z l = 2\Gamma. \tag{3.31}$$

The solution for small $\Gamma$ is

$$k_z = k_{z,n} = \frac{\pi}{l} n, \tag{3.32}$$

where $n = 0, \pm 1, \pm 2, \ldots$ . If we expand the trigonometric functions in Eq. (3.30) around $k_{z,n}$, we obtain

$$\frac{1}{2}\sin 2k_z l \approx \Gamma_{\perp,n} + (k_z - k_{z,n}) l, \tag{3.33}$$

$$\sin^4 k_z l \approx \Gamma^4_{\perp,n}, \tag{3.34}$$

where

$$\Gamma_{\perp,n} = \frac{k_{z,n}}{\eta k^2}. \tag{3.35}$$

Substituting Eqs. (3.32)–(3.34) into Eq. (3.30), we obtain

$$|\mathscr{L}_{\perp}(\mathbf{k})|^2 = \sum_{n=-\infty}^{\infty} \frac{\Gamma^2_{\perp,n}}{(k_z - k_{z,n})^2 l^2 + \Gamma^4_{\perp,n}}. \tag{3.36}$$

When $\eta\to\infty$, the Lorentzian functions in Eq. (3.36) become $\delta$ functions so that

$$\lim_{\eta\to\infty} |\mathscr{L}_{\perp}(\mathbf{k})|^2 = \frac{\pi}{l} \sum_{n=-\infty}^{\infty} \delta(k_z - k_{z,n}). \tag{3.37}$$

Repeating the same analysis for $|\mathscr{L}_{\parallel}|^2$, we obtain

$$|\mathscr{L}_{\parallel}(\mathbf{k})|^2 = \sum_{n=-\infty}^{\infty} \frac{\Gamma^2_{\parallel,n}}{(k_z - k_{z,n})^2 l^2 + \Gamma^4_{\parallel,n}}, \tag{3.38}$$

where

$$\Gamma_{\parallel,n} = \frac{1}{\eta k_{z,n}}. \tag{3.39}$$

Again, when $\eta\to\infty$, the Lorentzian functions in Eq. (3.38) become $\delta$ functions, thus

$$\lim_{\eta\to\infty} |\mathscr{L}_{\parallel}(\mathbf{k})|^2 = \frac{\pi}{l} \sum_{n=-\infty}^{\infty} \delta(k_z - k_{z,n}). \tag{3.40}$$

From Eqs. (3.8)–(3.10), (3.26)–(3.28), (3.37), and (3.40) we see that, in the limit where $\eta\to\infty$, Eq. (3.25) yields [the negative values of $n$ in the infinite sums in Eqs. (3.37) and (3.40) do not contribute because the integral in Eq. (3.7) is restricted to $k_z \geqslant 0$]

$$\lim_{\eta\to\infty} \mathbf{E}^{+}_{\mathrm{cav}}(\mathbf{r}) = i \frac{\pi}{l} \sum_{n=0}^{\infty} \int d^2\kappa \mathscr{E}_{\mathrm{vac}} e^{i\boldsymbol{\kappa}\cdot\mathbf{r}} \Big[ \hat{\mathbf{z}} \wedge \hat{\boldsymbol{\kappa}} A_{\perp}(k_{z,n}\hat{\mathbf{z}} + \boldsymbol{\kappa}) \times \sin k_{z,n} z + \Big( \hat{\boldsymbol{\kappa}} \frac{k_{z,n}}{k} \sin k_{z,n} z + i\hat{\mathbf{z}} \frac{\kappa}{k} \cos k_{z,n} z \Big) A_{\parallel}(k_{z,n}\hat{\mathbf{z}} + \boldsymbol{\kappa}) \Big]. \tag{3.41}$$

We must now determine the commutation relations satisfied by the operators $A_\perp(k_{z,n}\hat{\mathbf{z}}+\boldsymbol{\kappa})$ and $A_\parallel(k_{z,n}\hat{\mathbf{z}}+\boldsymbol{\kappa})$. If we substitute Eq. (3.23) into the commutation relation (3.18), we obtain

$$[A_\perp(\mathbf{k}),A_\perp^\dagger(\mathbf{k}')]\mathscr{E}_\perp^*(\mathbf{k})\mathscr{E}_\perp(\mathbf{k}')=\delta(\mathbf{k}'-\mathbf{k}). \quad (3.42)$$

Multiplying both sides by $\mathscr{E}_\perp(\mathbf{k})\mathscr{E}_\perp^*(\mathbf{k}')$ and taking the limit $\eta\to\infty$, we find

$$\frac{\pi}{l}\sum_{n,n'}\delta(k_z-k_{z,n})\,\delta(k_z'-k_{z,n'})[A_\perp(\mathbf{k}),A_\perp^\dagger(\mathbf{k}')]$$
$$=\sum_m\delta(k_z-k_{z,m})\,\delta(\mathbf{k}'-\mathbf{k}). \quad (3.43)$$

If we now integrate Eq. (3.43) over $k_z$ from $k_{z,n}-\epsilon$ to $k_{z,n}+\epsilon$ and over $k_z'$ from $k_{z,n'}-\epsilon$ to $k_{z,n'}+\epsilon$, with $\epsilon$ being small enough to include only $k_{z,n}$ and $k_{z,n'}$, we obtain

$$[A_\perp(k_{z,n}\hat{\mathbf{z}}+\boldsymbol{\kappa}),A_\perp^\dagger(k_{z,n'}\hat{\mathbf{z}}+\boldsymbol{\kappa})]$$
$$=\frac{l}{\pi}\delta(\boldsymbol{\kappa}'-\boldsymbol{\kappa})\int_{k_{z,n'}-\epsilon}^{k_{z,n'}+\epsilon}dk_z'\,\delta(k_z'-k_{z,n})$$
$$=\frac{l}{\pi}\delta(\boldsymbol{\kappa}'-\boldsymbol{\kappa})\,\delta_{n',n}. \quad (3.44)$$

So, apart from a normalization factor of $\sqrt{\pi/l}$, the operator $A_\perp(k_{z,n}\hat{\mathbf{z}}+\boldsymbol{\kappa})$ behaves as a continuous annihilation operator in $\boldsymbol{\kappa}$ and as a discrete annihilation operator in $k_z$. For this reason, we make a slight change of notation, defining

$$a_{\perp,n}(\boldsymbol{\kappa})\equiv\sqrt{\frac{\pi}{l}}A_\perp(k_{z,n}\hat{\mathbf{z}}+\boldsymbol{\kappa}), \quad (3.45)$$

where

$$[a_{\perp,n}(\boldsymbol{\kappa}),a_{\perp,n'}^\dagger(\boldsymbol{\kappa}')]=\delta_{n',n}\delta(\boldsymbol{\kappa}'-\boldsymbol{\kappa}). \quad (3.46)$$

Moreover, from Eq. (3.17), we obtain

$$[a_{\perp,n}(\boldsymbol{\kappa}),a_{\perp,n'}(\boldsymbol{\kappa}')]=0. \quad (3.47)$$

Similarly, for $A_\parallel(k_{z,n}\hat{\mathbf{z}}+\boldsymbol{\kappa})$ we find

$$[a_{\parallel,n}(\boldsymbol{\kappa}),a_{\parallel,n'}^\dagger(\boldsymbol{\kappa}')]=\delta_{n',n}\delta(\boldsymbol{\kappa}'-\boldsymbol{\kappa}), \quad (3.48)$$

$$[a_{\parallel,n}(\boldsymbol{\kappa}),a_{\parallel,n'}(\boldsymbol{\kappa}')]=0, \quad (3.49)$$

where $a_{\parallel,n}(\boldsymbol{\kappa})$ is defined by

$$a_{\parallel,n}(\boldsymbol{\kappa})\equiv\sqrt{\frac{\pi}{l}}A_\parallel(k_{z,n}\hat{\mathbf{z}}+\boldsymbol{\kappa}). \quad (3.50)$$

Expressing $A_\perp(k_{z,n}\hat{\mathbf{z}}+\boldsymbol{\kappa})$ and $A_\parallel(k_{z,n}\hat{\mathbf{z}}+\boldsymbol{\kappa})$ in terms of the annihilation operators $a_{\perp,n}(\boldsymbol{\kappa})$ and $a_{\parallel,n}(\boldsymbol{\kappa})$, we obtain [50]

$$\lim_{\eta\to\infty}\mathbf{E}_{\rm cav}^+(\mathbf{r})=i\sqrt{\frac{\pi}{l}}\sum_{n=0}^\infty\int d^2\kappa\,\mathscr{E}_{\rm vac}e^{i\boldsymbol{\kappa}\cdot\mathbf{r}}\Bigg[\hat{\mathbf{z}}\wedge\hat{\boldsymbol{\kappa}}\hat{a}_\perp(\boldsymbol{\kappa})\sin k_{z,n}z$$
$$+\left(\hat{\boldsymbol{\kappa}}\frac{k_{z,n}}{k}\sin k_{z,n}z+i\hat{\mathbf{z}}\frac{\kappa}{k}\cos k_{z,n}z\right)a_\parallel(\boldsymbol{\kappa})\Bigg]. \quad (3.51)$$

Before we return to the finite reflectivity case, it is interesting to study the changes in spontaneous emission induced by such a perfect parallel plates cavity. We notice that because there is still a continuum of modes available, an atom will always be in the weak-coupling regime in such a cavity. The mode structure, however, is radically different from that of the free space; the cavity only allows modes with certain discrete values of the component of the wave vector normal to the plates. So spontaneous emission will remain an irreversible exponential decay process, but the decay rate can be dramatically different from that of free space. We will now calculate this decay rate for a single atom inside the cavity, in the two-level atom and dipole approximations [51].

As we are in the weak-coupling regime, we can use Fermi's golden rule to compute the spontaneous-emission decay rate $\gamma$ in the cavity and find

$$\gamma=\frac{2\pi}{\hbar^2}\int dk^3\sum_{\alpha=\perp,\parallel}|\langle\downarrow,\mathbf{k},\alpha|\mathbf{d}\cdot\mathbf{E}_{\rm cav}(\mathbf{r}_a)|\uparrow,0\rangle|^2$$
$$\times\delta(\omega-\omega_a), \quad (3.52)$$

where $\mathbf{r}_a$ is the position of the atom in the cavity, $\omega_a$ is the atomic transition frequency, $\mathbf{d}$ is the atomic dipole operator, $|\downarrow,\mathbf{k},\alpha\rangle$ is the state in which the atom is not excited and the field mode $\mathbf{k}$ of polarization $\alpha$ has one photon, all the other modes having no photons, and the state $|\uparrow,0\rangle$ is the state in which the atom is excited and the field has no photons. Let us consider the case where the atomic dipole is parallel to the plates. After substituting Eq. (3.51) in Eq. (3.52), we obtain

$$\gamma_\rho=\frac{\omega_a d^2}{2\pi\varepsilon_0\hbar l}\sum_{n=0}^\infty\int_0^{2\pi}d\phi\int_0^\infty\kappa d\kappa\left[\frac{c\pi n}{\omega_a l}\cos\phi-\sin\phi\right]^2$$
$$\times\sin^2\left(\frac{n\pi}{l}z_a\right)\delta(\omega-\omega_a). \quad (3.53)$$

The angular integration yields

$$\gamma_\rho=\frac{\omega_a d^2}{2\varepsilon_0\hbar l}\sum_{n=0}^\infty\int_0^{2\pi}d\phi\int_0^\infty\kappa d\kappa\left[\left(\frac{c\pi n}{\omega_a l}\right)^2-1\right]$$
$$\times\sin^2\left(\frac{n\pi}{l}z_a\right)\delta(\omega-\omega_a). \quad (3.54)$$

For any differentiable function $y(x)$ with an inverse $x(y)$ and any function $g(x)$ we have

$$\int dx\;g(x)\,\delta(y(x))=\int dy\;g(x(y))\frac{\delta(y)}{dy/dx}. \quad (3.55)$$

Using (3.55), we can change the variable of integration in Eq. (3.54) to $\omega$, recovering the well-known [50] expression

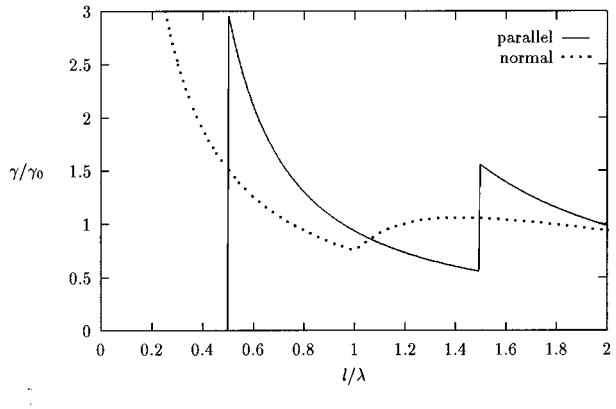


FIG. 6. Plot of the decay rate of an atom between two perfect mirrors as a function of mirror separation. The full line corresponds to an atom with its electric-dipole moment parallel to the mirrors and the dotted line to a dipole moment normal to the mirrors. The decay rates are given in units of the decay rate in free space and the mirror separation in units of the atomic transition wavelength.

for the decay rate of an atom between two perfect mirrors with a dipole moment parallel to the mirrors:

$$\gamma_\rho=\gamma_0\sum_{n=0}^{[2l/\lambda]}\frac{3\lambda}{4l}\left\{1+\left(\frac{n\lambda}{2l}\right)^2\right\}\sin^2\left(\frac{n\pi}{l}z_a\right), \quad (3.56)$$

where $[2l/\lambda]$ is the largest integer number of half wavelengths of the atomic transition that can fit in the plate separation $l$ and $\gamma_0$ is the free space decay rate given by

$$\gamma_0=\frac{\omega_a^3 d^2}{3\pi\hbar\varepsilon_0 c^3}. \quad (3.57)$$

For a dipole normal to the plates, a similar calculation yields the well-known [50] result

$$\gamma_z=\gamma_0\left\{\frac{3\lambda}{4l}+\sum_{n=1}^{[2l/\lambda]}\frac{3\lambda}{2l}\left[1-\left(\frac{n\lambda}{2l}\right)^2\right]\cos^2\left(\frac{n\pi}{l}z_a\right)\right\}. \quad (3.58)$$

In Fig. 6, we plot the decay rates, given by (3.56) and (3.58), for an atom at the center of the cavity as a function of the plate separation $l$ [50]. We notice that there is no spontaneous emission when the dipole is parallel to the plates and the plate separation is narrower than half the atomic wavelength. The reason is that at wavelengths larger than $2l$, the only modes available are those where $n=0$ whose polarizations are normal to the plates and therefore not interacting with the dipole. Another way of understanding this is to think of the images of the dipole on the plates [52–56] drawing an analogy with many-atom cooperative decay [57]. When the dipole is parallel to the plates and the plate separation is shorter than half the atomic wavelength, the radiation emitted by each image adds up to cancel completely the radiation emitted by the real dipole. Then we see that complete inhibition of spontaneous emission can only happen when the plates are perfect reflectors. Any small transmissivity would upset this delicate balance between the images and the dipole, allowing some degree of spontaneous emission in the cavity. We will return to this point in Sec. IV.

There is no such complete inhibition of spontaneous emission for a dipole normal to the plates because then the dipole will interact with the $n=0$ modes. This is also the reason why $\gamma_z$ diverges in Fig. 6 when the plate separation decreases to zero. Because the energy density in the $n=0$ vacuum modes is inversely proportional to the volume between the plates when the plate separation decreases, the coupling with the field increases, leading to the divergence. Before such a divergence occurs, the interaction between the atom and the atoms on the surface of the plates, which we have neglected in this simple model, should become important. In the next section we see that when the top plate is no longer a perfect reflector, $\gamma_\rho$ will also display such a divergence.

## IV. SPONTANEOUS-EMISSION RATE

In this section we investigate how the spontaneous-emission rate changes when the finesse of the cavity increases [26]. Let us start by considering the case of very low finesse where the top mirror is almost completely transparent. Then we can assume that $\eta$ is much smaller than the atomic wavelength so that

$$\Lambda_a=\frac{\omega_a}{c}\eta\ll 1. \quad (4.1)$$

We will now calculate the spontaneous-emission rate up to first order in $\Lambda_a$.

For a dipole normal to the plates, Eqs. (3.7) and (3.52) yield, up to first order in $\Lambda_a$

$$\gamma_z=\frac{\omega_a^3 d^2}{\pi\varepsilon_0\hbar c^3}\int_0^1 dx\left(1+\Lambda_a x\,\sin 2\frac{\omega_a}{c}lx\right)(1-x^2)\cos^2\frac{\omega_a}{c}zx. \quad (4.2)$$

This integral can be solved analytically for the general case; however, it is more instructive to consider special cases.

First we notice that when $\Lambda_a$ vanishes, Eq. (4.2) reduces to

$$\gamma_z=3\gamma_0\left[\frac{1}{3}-\left(\frac{c}{\omega_a z}\right)^2\cos 2\frac{\omega_a}{c}z+\left(\frac{c}{\omega_a z}\right)^3\cos 2\frac{\omega_a}{c}z\right]. \quad (4.3)$$

This is the well-known expression for the spontaneous-emission decay rate of an atom near a perfect mirror when the atomic dipole is normal to the mirror [52,58,50]. As we can see from Eq. (4.3), we do not need a cavity to change the spontaneous emission rate. In fact, the first controlled experimental study of modified spontaneous emission [59] concerned the fluorescence of dye molecules near a single mirror.

In order to study the effect of the top mirror we must take $\Lambda_a\neq 0$ in Eq. (4.2). Let us do so and compute the first-order cavity effects. Consider a half wavelength cavity. When both plates are perfect reflectors, the spontaneous-emission rate is three-halves of that in free space at any point inside the cavity for a dipole normal to the plates. So our first-order correction will depend on the position and for each position it will be a correction in the direction that will bring the

single mirror decay rate given by (4.3) closer to the constant rate of three-halves of the rate in free space. In fact, after some lengthy algebra, we find that when the atom is at the center of the cavity, Eq. (4.2) yields

$$\gamma_z = 3\gamma_0\left\{\frac{1}{3}+\frac{1}{\pi^2}+\frac{\omega_a\eta}{c}\frac{85}{72\pi^3}\right\}, \tag{4.4}$$

so that the semitransparent mirror enhances spontaneous emission to bring it closer to three-halves of $\gamma_0$. On the other hand, when the atom sits on the perfect mirror, we find

$$\gamma_z = 3\gamma_0\left\{\frac{2}{3}-\frac{\omega_a\eta}{c}\frac{3}{2\pi^3}\right\} \tag{4.5}$$

and the semitransparent mirror inhibits spontaneous emission, again bringing it closer to three-halves of $\gamma_0$. Similar results can be shown for $\gamma_\rho$.

Let us now consider the case of a highly reflective top mirror. Substituting Eqs. (3.36) and (3.38) in (3.7) and then in (3.52), we obtain for a dipole parallel to the plates

$$\gamma_\rho = \frac{3}{2}\gamma_0\int_0^1 d(\cos\theta)\sum_{n=0}^{[2l/\lambda]}\left\{\frac{\Gamma_{\parallel,n}^2}{(k_z-k_{z,n})^2l^2+\Gamma_{\parallel,n}^4}\cos^2\theta + \frac{\Gamma_{\perp,n,a}^2}{(k_z-k_{z,n})^2l^2+\Gamma_{\perp,n,a}^4}\right\}\sin^2 k_z z, \tag{4.6}$$

where $\Gamma_{\parallel,n}$ is given by Eq. (3.39) and $\Gamma_{\perp,n,a}$ by

$$\Gamma_{\perp,n,a} = \frac{k_{z,n}c^2}{\eta\omega_a^2}. \tag{4.7}$$

When the plate separation is only a few atomic wavelengths and $\eta$ is much larger than the atomic wavelength, we can approximate both $\Gamma_{\parallel,n}$ and $\Gamma_{\perp,n,a}$ by

$$\Gamma_{\parallel,n}\approx\Gamma_{\perp,n,a}\approx\frac{c}{\eta\omega_a}\equiv\Gamma_a. \tag{4.8}$$

Here we have to be careful because unless $\eta\to\infty$, $\Gamma_{\parallel,0}$ will diverge, as can be seen from Eq. (3.39). As we have mentioned before, this means that $\mathscr{S}_\parallel$ does not have a resonance at $n=0$ unless $\eta\to\infty$. It is a consequence of the fact that the semitransparent mirror will not reflect radiation that is incident at an angle of $\pi/2$ with the normal except in the perfect mirror limit. There is no problem, however, in replacing $\Gamma_{\parallel,0}$ by $\Gamma_a$ because $|\mathscr{S}_\parallel|^2$ appears in Eq. (4.6) multiplied by $\cos^2\theta$ so that, in this case, the $n=0$ Lorentzian function will vanish giving no contribution in Eq. (4.9). Then Eq. (4.6) becomes

$$\gamma_\rho = \frac{3}{2}\gamma_0\int_0^1 dx\sum_{n=0}^{[2l/\lambda]}\frac{\Gamma_a^2}{(\omega_a x/c-k_{z,n})^2l^2+\Gamma_a^4} \times(x^2+1)\sin^2\frac{\omega_a}{c}zx. \tag{4.9}$$

If we now write the sine function as a sum of exponentials and extend the integration to the entire $x$ axis (when $\Gamma_a$ is much smaller than one, the part of the integration over the tails of the Lorentzian functions will give a negligible contribution to the total integral), we obtain

$$\gamma_\rho = \frac{3\lambda}{8l}\gamma_0\sum_{n=0}^{[2l/\lambda]}\left\{\left(\frac{n\lambda}{2l}\right)^2+1\right\}\left\{1-e^{-2z\Gamma_a^2/l}\cos\left(2\pi n\frac{z}{l}\right)\right\}, \tag{4.10}$$

where again $[2l/\lambda]$ is the maximum integer number of half atomic wavelengths $\lambda$ that can fit the plate separation $l$.

A similar calculation yields the following expression for the spontaneous-emission rate in the high reflectivity limit when the atomic dipole is normal to the plates:

$$\gamma_z = \frac{3\lambda}{4l}\gamma_0\left\{1+\sum_{n=1}^{[2l/\lambda]}\left[1-\left(\frac{n\lambda}{2l}\right)^2\right]\times\left[1+e^{-2z\Gamma_a^2/l}\cos\left(2\pi n\frac{z}{l}\right)\right]\right\}. \tag{4.11}$$

Comparing Eqs. (4.10) and (4.11) with the corresponding expressions for two perfectly reflecting parallel plates (3.56) and (3.58), we notice the only difference is the decaying exponentials in Eqs. (4.10) and (4.11) that stem from the transparency of the upper mirror. This does not bring any significant differences from the perfect mirror case for a dipole normal to the mirrors. For a dipole parallel to the mirrors, however, we notice the dramatic change mentioned in Sec. III B. This is shown in Fig. 7, where we plot the ratio $\gamma_\rho/\gamma_0$ given by Eq. (4.10) as a function of the plate separation in units of atomic wavelengths for an atom at the center of the cavity. We can see from Fig. 7 that as long as there is at least a small amount of cavity loss due to mirror transmissivity, spontaneous-emission will not be completely suppressed. In other words, this means that when the upper mirror is not a perfect reflector, there will be modes, other than the $k_z=0$ modes, whose frequencies lie within the atomic resonance and whose polarization is not orthogonal to the atomic dipole.

Finally, we discuss the spontaneous-emission rate for a $\lambda/2$ cavity when the atomic dipole is parallel to the plates.

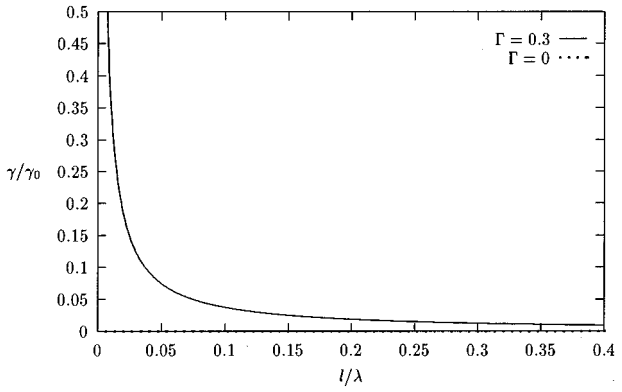


FIG. 7. Plot of the spontaneous-emission rate in units of the rate in free space as a function of plate separation for an atom at the center of the cavity with its dipole moment parallel to the mirrors. The dotted line correspond to the case where both mirrors are perfect ($\Gamma_a=0$) and the full line to the case where $\Gamma_a=0.3$.

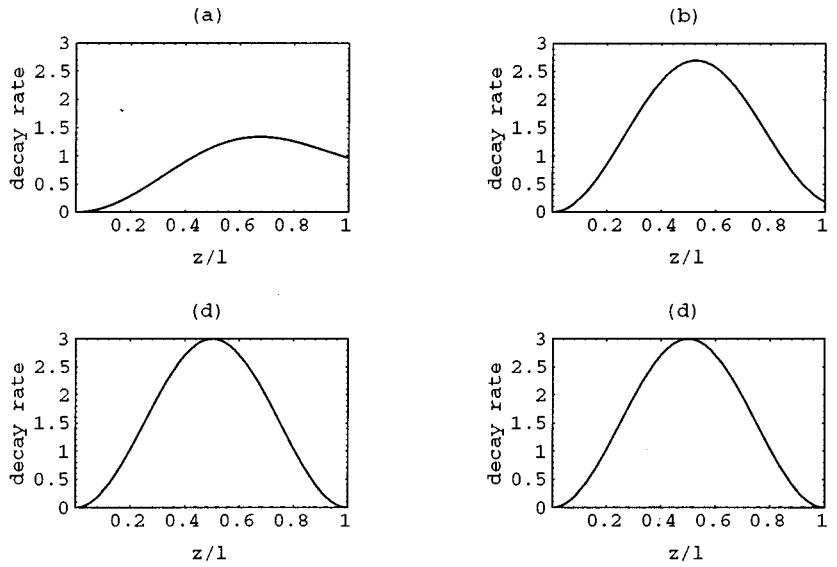


FIG. 8. Plot of the decay rate, in units of the free-space decay rate, as a function of the position of the atom. In (a) we show the case of a single perfect mirror. In (b) we show the case of a half wavelength cavity with $\Lambda_a=1$. In (c) we repeat the plot for the same cavity but with a much higher finesse ($\Lambda_a=10^3$). In (d) we show the case of two perfect mirrors for comparison.

This is the case where an atom with a sufficiently narrow (a linewidth smaller than $\pi/l$) atomic line will couple to the $(n=1)$ cavity resonance only. In Fig. 8 we plot the ratio of the decay rate in the cavity to that in free space as a function of the position of the atom for four different finesses. We see that when the reflectivity of the upper mirror is low, spontaneous emission is not suppressed on the upper mirror and the maximum rate is not exactly at the center and is less than three times the rate in free space. As the reflectivity increases, the maximum rate increases towards three times that in free space and becomes very small on the upper mirror.

## V. VACUUM FLUCTUATIONS

Vacuum fluctuations play an important role in the spontaneous-emission process [60,61]. In free space, such fluctuations are isotropic. A cavity, however, modifies the mode structure of its surrounding space, leading to different vacuum fluctuations. We show in this section that our planar microcavity introduces a preferred direction, the direction normal to the plates, radically changing the vacuum fluctuations associated with emission in this direction (for two perfect mirrors, this directionality has already been investigated within the framework of classical antenna theory and the image method [56]). As a result, spontaneous emission will become anisotropic [23]. This anisotropy can be used to increase the probability of spontaneous emission in a particular direction. In a laser, if this particular direction is chosen to be the direction where laser light is generated, most of the photons produced by spontaneous emission would go into the lasing modes instead of being wasted to other modes and the threshold would be reduced [21,22,62,63].

In general, atoms are more strongly affected by the component of the electric field in the direction of its electric dipole [48]. We consider here the case where the atomic dipole is parallel to the mirrors and choose the $x$ axis to be in the direction of the dipole. We examine the vacuum field fluctuations in the $x$ component of the electric field, whose variance provides a good measure of these fluctuations. We notice, however, that for this given polarization ($x$ component of the electric field) and frequency (atomic resonance), there are, in general, several modes of the field, one for each wave vector $\mathbf{k}$. We have devised a way of plotting the variance, at a given position in space, of each mode corresponding to this chosen polarization and frequency: we plot the surface spanned by a vector whose direction coincides with that of a wave vector $\mathbf{k}$ and whose length gives the variance of the corresponding mode. The advantage of plotting this way is that for any given mode whose variance is shown in the graph, we can immediately see what is the direction of emission for emission in that mode. The variance of a mode at a given position is a measure of how likely is an atom occupying that position to emit in that mode. This kind of plot will automatically show in which directions an atom sitting at a given position will be more likely to emit, making any anisotropy explicitly evident in the graph. As an illustration, we plot in Fig. 9 the variance of the $x$ component of the electric field at a given frequency $\omega$ in free space, given by

$$[\Delta E_x^{\text{free}}(\mathbf{r},\mathbf{k})]^2=\frac{1}{4}\frac{\hbar\omega}{4\pi^3\varepsilon_0}[1-(\hat{\mathbf{k}}\cdot\hat{\mathbf{x}})^2]. \tag{5.1}$$

We notice that this variance is almost isotropic except that the constraint $\mathbf{E}\cdot\mathbf{k}=0$ makes it look rather like a doughnut, with a hole in the middle because the $x$ component of the electric field gets smaller and smaller as $\mathbf{k}$ approaches the $x$ axis.

Now let us examine how these fluctuations change when we are in a cavity. We consider a cavity whose length is half of the wavelength of the atomic transition and we will compute the variance at the center of the cavity. In a one-dimensional model with perfect mirrors, this would correspond to the case where the cavity supports a single mode only, whose maximum is at the center of the cavity.

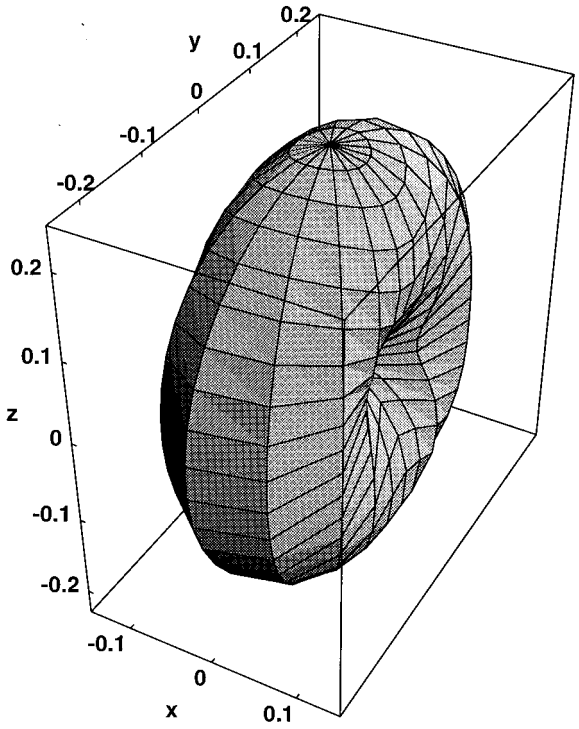


FIG. 9. Variance (in units of $\hbar ck/4\pi^3\varepsilon_0$) of the $x$ component of the electric field plotted for each mode of frequency $ck$ as the length of the vector from the origin that points to the surface in the figure in the direction $\hat{\mathbf{k}}$ of the mode. The toroidal shape appears because of the polarization constraint $\mathbf{E}\cdot\hat{\mathbf{k}}=0$.

From Eq. (3.7) we obtain the following expression for the variance of mode $\mathbf{k}$ at position $\mathbf{r}$ inside the cavity

$$[\Delta E_x(\mathbf{r},\mathbf{k},t)]^2=\frac{\hbar\omega}{4\pi^3\varepsilon_0}[|\mathscr{G}_{\parallel}(\mathbf{k})|^2\cos^2\theta\,\cos^2\phi + |\mathscr{G}_{\perp}(\mathbf{k})|^2\sin^2\phi]\sin^2 k_z z. \tag{5.2}$$

The variance in the presence of a single perfect mirror changes with the nature of the semitransparent mirror above it forming the top of the cavity. For a perfect mirror alone, i.e., $\eta=0$, the fluctuations are constrained to the half space but are still quite isotropic, as can be seen in Fig. 10. When the semitransparent upper mirror is present as well, i.e., $\eta\neq 0$, we notice a substantial increase in the fluctuations in the $z$ direction, perpendicular to the mirrors, as we can see in Fig. 11. As the reflectivity increases, i.e., when $\eta$ increases, this anisotropy becomes more pronounced. In Fig. 12 we compare plots for increasing values of $\eta$ to show how the fluctuations tend to dominate around the $z$ direction as the reflectivity increases. As the reflectivity increases, we approach the results of Dowling *et al.* [56] obtained for two perfect mirrors.

We have also examined the fluctuations at other positions inside the cavity as well as for other cavity lengths. However, the case discussed above seems to be the most interesting because it is the case where an atom with a sufficiently narrow (a linewidth much smaller than $\pi/l$) atomic line will couple to the $(n=1)$ cavity resonance only.

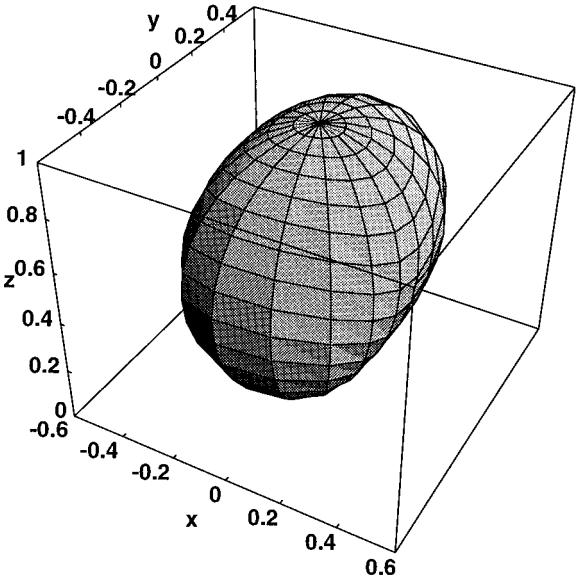


FIG. 10. Variance of the $x$ component of the electric field (in units of $\hbar\omega/4\pi^3\varepsilon_0$) for an atom in front of a single mirror with the atomic dipole moment parallel to the mirror. The perfect mirror divides space into two halves destroying the toroidal shape we have seen for free space. We notice that the maximum value of the variance in this case is four times larger than the maximum value in free space.

## VI. SPONTANEOUS-EMISSION PATTERN

We have been concerned so far only with the radiation inside the cavity. This cavity, however, can let some of the radiation escape outside when the upper mirror is not a perfect reflector. In this section we shall venture outside the cavity and study the radiation that leaks out. We will consider the simplest possible case where there is a single atom in the cavity. We will then calculate the field outside produced by the spontaneous emission of the atom inside the cavity. A similar calculation was also performed by De Martini *et al.* [49]. Their calculation, however, only yields the electric field along a line normal to the mirrors passing through the atom and does not describe the dependence of the field on the $x$ and $y$ coordinates. We will obtain such dependence explicitly. This will lead to a curious result that shows how the anisotropy of spontaneous emission in the cavity, discussed in the preceding section, manifests itself outside the cavity.

In the interaction picture, the positive-frequency component of the electric field outside the microcavity (3.7) is given by

$$\mathbf{E}^{+}_{\mathrm{out}}(\mathbf{r})=\int d^3k\; e^{-i\omega t}\{\mathscr{E}^{\mathrm{out}}_{\perp}(\mathbf{r},\mathbf{k})\hat{\mathbf{e}}_{\perp}(\mathbf{k})a_{\perp}(\mathbf{k}) + [\mathscr{E}^{\mathrm{out}}_{\parallel,1}(\mathbf{r},\mathbf{k})\hat{\mathbf{e}}_{\parallel,1}(\mathbf{k})+\mathscr{E}^{\mathrm{out}}_{\parallel,2}(\mathbf{r},\mathbf{k})\hat{\mathbf{e}}_{\parallel,2}(\mathbf{k})]a_{\parallel}(\mathbf{k})\}. \tag{6.1}$$

In order to calculate $\mathbf{E}^{+}_{\mathrm{out}}$ we must find how the time evolution of annihilation operators in Eq. (6.1) is affected by the interaction with the atom in the cavity.

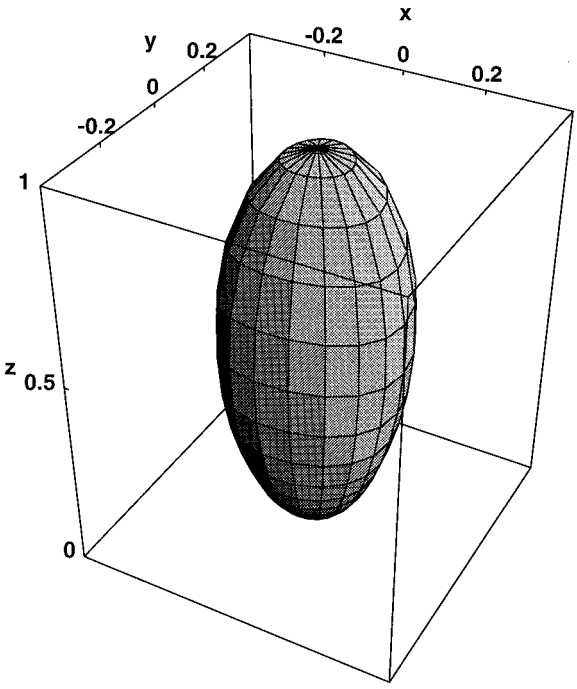


FIG. 11. Variance of the $x$ component of the electric field (in units of $\hbar\omega/4\pi^3\varepsilon_0$) for an atom between two parallel mirrors, the lower one being a perfect mirror and the upper one semitransparent with $\Lambda_a=1$. We notice that emission is much more directional here than it is for free space or for a single mirror.

For an atom at $\mathbf{r}_a$ with a dipole parallel to the mirrors (along the $x$ axis), we obtain the following equation of motion for the annihilation operators:

$$\frac{d}{dt}a_\alpha(\boldsymbol{\kappa})=i\mu\mathscr{E}_\alpha^{\mathrm{cav}*}(\mathbf{r}_a,\mathbf{k})\hat{\mathbf{x}}\cdot\hat{\mathbf{e}}_\alpha(\hat{\mathbf{k}})e^{i(\omega-\omega_a)t}\sigma(t), \quad (6.2)$$

where $\mu$ is the transition dipole moment of the atom, $\alpha=\perp,\parallel$, and $\sigma$ is the lowering atomic operator. Because this microcavity does not confine the field in all three spatial dimensions, but only in one dimension, there are no Rabi oscillations [64] and the time evolution of the atomic lowering operator is given, to a reasonably good approximation [49], by the modified Weisskopf-Wigner exponentially decaying solution

$$\sigma(t)=\sigma(0)e^{-(i\omega_a+\gamma/2)t}+\mathscr{L}_\sigma, \quad (6.3)$$

where $\mathscr{L}_\sigma$ is the Langevin noise term associated with the dipole coupling to the vacuum field (needed to preserve the commutation relations of the operators). The precise form of $\mathscr{L}_\sigma$ is unimportant because we do not study here the noise properties of the emitted light. The decay constant $\gamma$ is the cavity-modified spontaneous-emission decay rate at the position of the atom given by

$$\gamma=\frac{\mu^2}{2\pi^2\hbar\epsilon_0}\int\omega d^3k[|\mathscr{L}_\parallel(\mathbf{k})|^2\cos^2\phi\,\cos^2\theta + |\mathscr{L}_\perp(\mathbf{k})|^2\sin^2\phi]\delta(\omega-\omega_a)\sin^2k_z z_a. \quad (6.4)$$

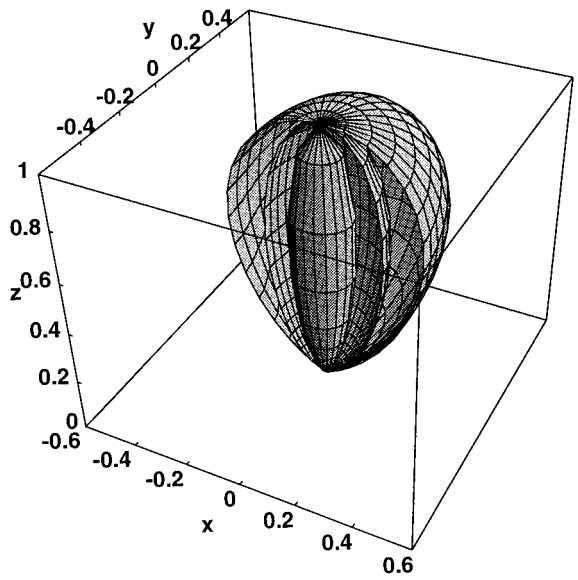


FIG. 12. Comparison between plots of the variance of the $x$ component of the electric field (in units of $\hbar\omega/4\pi^3\varepsilon_0$) for an atom with dipole moment parallel to the mirrors for increasing finesse. The more isotropic variance here is the one for a single mirror ($\Lambda_a=0$), then there is the one for $\Lambda_a=1$ and the case $\Lambda_a=5$ where emission is quite biased in the $z$ direction.

We can then integrate Heisenberg's equations for the field annihilation operators in the rotating-wave approximation and obtain the following expression for the field operators:

$$a_\alpha(\mathbf{k},t)=a_\alpha(\mathbf{k},0)e^{-i\omega t}+i\mu\mathscr{E}_\alpha^{\mathrm{cav}*}(\mathbf{r}_a,\mathbf{k})\hat{\mathbf{x}}\cdot\hat{\mathbf{e}}_\alpha(\mathbf{k}) \times\frac{e^{[i(\omega-\omega_a)-(\gamma/2)]t}-1}{i(\omega-\omega_a)-(\gamma/2)}e^{-i\omega t}\sigma(0), \quad (6.5)$$

where $\alpha=\perp,\parallel$. This is then inserted into the expression for the electric field outside the cavity (6.1), yielding

$$\mathbf{E}^+_{\mathrm{out}}(\mathbf{r},t)=\mathbf{E}^+_{\mathrm{vac,out}}(\mathbf{r},t)+\mathbf{E}^+_{s,\mathrm{out}}(\mathbf{r},t), \quad (6.6)$$

where the first term on the right-hand side is the cavity-modified vacuum

$$\mathbf{E}^+_{\mathrm{vac,out}}(\mathbf{r},t)=\int d^3k\; e^{-i\omega t}\{\mathscr{E}^{\mathrm{out}}_\perp(\mathbf{r},\mathbf{k})\hat{\mathbf{e}}_\perp(\hat{\mathbf{k}})a_\perp(\mathbf{k},0) +[\mathscr{E}^{\mathrm{out}}_{\parallel,1}(\mathbf{r},\mathbf{k})\hat{\mathbf{e}}_{\parallel,1}(\hat{\mathbf{k}}) +\mathscr{E}^{\mathrm{out}}_{\parallel,2}(\mathbf{r},\mathbf{k})\hat{\mathbf{e}}_{\parallel,2}(\hat{\mathbf{k}})]a_\parallel(\mathbf{k},0)\} \quad (6.7)$$

and the second term is the field emitted by the atom

$$\mathbf{E}^+_{s,\mathrm{out}}(\mathbf{r},t)=i\mu\sigma(0)e^{-i\omega_a t}\int d^3k\frac{e^{-\gamma t/2}-e^{-i(\omega-\omega_a)t}}{i(\omega-\omega_a)-\gamma/2} \times\mathscr{E}(\mathbf{k},\mathbf{r},\mathbf{r}_a), \quad (6.8)$$

with $\mathscr{E}$ given by

$$\mathscr{E}(\mathbf{k},\mathbf{r},\mathbf{r}_a)=\mathscr{E}_{\perp}^{\text{out}}(\mathbf{r},\mathbf{k})\mathscr{E}_{\perp}^{\text{cav}*}(\mathbf{r}_a,\mathbf{k})\hat{\mathbf{x}}\cdot\hat{\mathbf{e}}_{\perp}(\hat{\mathbf{k}})\hat{\mathbf{e}}_{\perp}(\hat{\mathbf{k}})$$
$$+[\mathscr{E}_{\|,1}^{\text{out}}(\mathbf{r},\mathbf{k})\hat{\mathbf{e}}_{\|,1}(\hat{\mathbf{k}})+\mathscr{E}_{\|,2}^{\text{out}}(\mathbf{r},\mathbf{k})\hat{\mathbf{e}}_{\|,2}(\hat{\mathbf{k}})]$$
$$\times[\mathscr{E}_{\|,1}^{\text{cav}*}(\mathbf{r}_a,\mathbf{k})\hat{\mathbf{x}}\cdot\hat{\mathbf{e}}_{\|,1}(\hat{\mathbf{k}})$$
$$+\mathscr{E}_{\|,2}^{\text{cav}*}(\mathbf{r}_a,\mathbf{k})\hat{\mathbf{x}}\cdot\hat{\mathbf{e}}_{\|,2}(\hat{\mathbf{k}})]. \tag{6.9}$$

As we are interested in the case where spontaneous emission is enhanced, we will consider the high reflectivity limit we have discussed in Sec. IV. In Sec. III B we have obtained approximate expressions for $|\mathscr{G}_{\perp}|^2$ and $|\mathscr{G}_{\|}|^2$ in the high reflectivity limit. In this section we will also need approximate expressions for the products of these functions with the factors linear in $\Lambda$ that appear in the mode functions $\mathscr{E}_{\alpha}^{\text{out}}$ in Eq. (6.9). Proceeding in the same way as we have in Sec. III B, we obtain, after some algebra, the following approximate expressions for these products:

$$|\mathscr{G}_{\|}(\mathbf{k})|^2\Lambda\ \cos\theta\ \sin\delta=\sum_{n=-\infty}^{\infty}\frac{(-1)^n\Gamma_{\|,n}^2}{(k_z-k_{z,n})^2l^2+\Gamma_{\|,n}^4}$$
$$\times\left\{1+\frac{l}{\Gamma_{\|,n}}(k_z-k_{z,n})\right\}, \tag{6.10}$$

$$|\mathscr{G}_{\perp}(\mathbf{k})|^2\frac{\Lambda\ \sin\delta}{\cos\theta}=\sum_{n=-\infty}^{\infty}\frac{(-1)^n\Gamma_{\perp,n}^2}{(k_z-k_{z,n})^2l^2+\Gamma_{\perp,n}^4}$$
$$\times\left\{1+\frac{l}{\Gamma_{\perp,n}}(k_z-k_{z,n})\right\}. \tag{6.11}$$

Let us now assume that the $n=1$ cavity resonance is only slightly (the detuning is much smaller than the mode separation $\pi/l$) detuned from the atomic transition wavelength. We also assume that the detuning is such that the atom is in the regime where spontaneous emission is enhanced. In other words, the atomic resonance is somewhere between the $n=1$ and the $n=2$ resonances, but much closer to $n=1$ than $n=2$ because the detuning is small. We can then neglect all the Lorentzians in Eqs. (3.36), (3.38), (6.10), and (6.11), except for the one where $n=1$. If we now make the change of variable $k\rightarrow k-k_a$ in the original integral over the wave number $k$ in Eq. (6.8) and extend the integration to the whole real axis as the tails of the Lorentzian functions give a negligible contribution to the integral, we notice that there are two kinds of integrals involved in that total integral. They have the forms

$$I_1=\int_{-\infty}^{\infty}dk\frac{(k+k_a)^3(e^{-\gamma t/2}-e^{-i\omega t})e^{iuk}\Gamma_{\alpha}'^2}{[k+i\gamma/2c][(k\ \cos\theta-k_c+k_a\cos\theta)^2l^2+\Gamma_{\alpha}'^4]}, \tag{6.12}$$

$$I_2=\int_{-\infty}^{\infty}dk\frac{(k+k_a)^3(k\ \cos\theta-k_c+k_a\cos\theta)(e^{-\gamma t/2}-e^{-i\omega t})e^{iuk}l\Gamma_{\alpha}'}{[k+i\gamma/2c][(k\ \cos\theta-k_c+k_a\cos\theta)^2l^2+\Gamma_{\alpha}'^4]}, \tag{6.13}$$

where $k_a$ is $2\pi$ over the wavelength of the atomic transition, $k_c=\pi/l$ is the $z$ component of the wave vector at the first cavity resonance (i.e., $k_{z,1}$), $\Gamma_{\alpha}'$ is $\Gamma_{\alpha}$ with $k$ replaced by $k+k_a$ ($\alpha=\perp,\|$) and $u$ is a function of $x$, $y$, $z$, $\theta$, and $\phi$. We will now examine each of these two integrals in turn, starting with $I_1$.

The integrand of $I_1$ has three poles given by

$$k_I=-i\frac{\gamma}{2c}, \tag{6.14}$$

$$k_{\pm}=k_c\sec\theta-k_a\pm i\frac{\Gamma_{\alpha}^2}{l}\sec\theta. \tag{6.15}$$

We can rewrite $I_1$ as a linear combination of two integrals

$$I_1=e^{-\gamma t/2}I_{11}-I_{12}. \tag{6.16}$$

Let us consider $I_{11}$ first. It is given by

$$I_{11}=\int_{-\infty}^{\infty}dk$$
$$\times\frac{e^{iuk}(\Gamma_{\alpha}'/l)^2(k+k_a)^3\sec^2\theta}{[k+i\gamma/2c][(k-k_c\sec\theta+k_a)^2-(\Gamma_{\alpha}'^2/l)^2\sec^2\theta]}. \tag{6.17}$$

For $u<0$, contour integration yields

$$I_{11}=2\pi i\left\{\frac{\Gamma_a^2e^{u\gamma/2c}[k_a-i\gamma/2c]^3}{([k_a-i\gamma/2c]\cos\theta-k_c)^2l^2+\Gamma_a^4}\right.$$
$$\left.+\frac{i}{2l}\frac{e^{i([k_c-i\Gamma_a^2/l]\sec\theta-k_a)u}(k_c-i\Gamma_a^2/l)^3\sec^4\theta}{(k_c-i\Gamma_a^2/l)\sec\theta-k_a+i\gamma/2c}\right\}, \tag{6.18}$$

and for $u>0$,

$$I_{11}=\frac{\pi}{l}\frac{e^{i([k_c+i\Gamma_a^2/l]\sec\theta-k_a)u}(k_c+i\Gamma_a^2/l)^3\sec^4\theta}{(k_c+i\Gamma_a^2/l)\sec\theta-k_a+i\gamma/2c}, \tag{6.19}$$

where we have assumed that $k_a$ and $k_c$ are much larger than $1/\eta$ and $\gamma/2c$ so that $\Gamma'_\alpha$ can be approximated by $\Gamma_a = 1/\eta k_a$ after the integration.

The second integral $I_{12}$ is given by

$$I_{12} = \int_{-\infty}^{\infty} dk \times \frac{(k+k_a)^3 e^{i(u-ct)k} (\Gamma'^2_\alpha/l)^2 \sec^2\theta}{[k+i\gamma/2c][(k-k_c\sec\theta+k_a)^2-(\Gamma'^2_\alpha/l)^2\sec^2\theta]}. \tag{6.20}$$

Contour integration of $I_{12}$ for $u<ct$ yields

$$I_{12} = 2\pi i \left\{ \frac{\Gamma_a^2 e^{(u-ct)\gamma/2c}[k_a - i\gamma/2c]^3}{([k_a - i\gamma/2c]\cos\theta - k_c)^2 l^2 + \Gamma_a^4} + \frac{i}{2l} \frac{e^{i([k_c - i\Gamma_a^2/l]\sec\theta - k_a)(u-ct)}(k_c - i\Gamma_a^2/l)^3 \sec^4\theta}{(k_c - i\Gamma_a^2/l)\sec\theta - k_a + i\gamma/2c} \right\}, \tag{6.21}$$

and for $u>ct$,

$$I_{12} = \frac{\pi}{l} \frac{e^{i([k_c + i\Gamma_a^2/l]\sec\theta - k_a)(u-ct)}(k_c + i\Gamma_a^2/l)^3 \sec^4\theta}{(k_c + i\Gamma_a^2/l)\sec\theta - k_a + i\gamma/2c}. \tag{6.22}$$

Let us now consider what will happen when $I_1$ is integrated over $\theta$. Here we have to remember that $u$ is a linear combination of $\cos\theta$ and $\sin\theta$. Let us examine the part of the integral that contains factors of the kind

$$\frac{1}{(k_c \pm \Gamma_a/l)\sec\theta - k_a + i\gamma/2c}. \tag{6.23}$$

If the width of this resonance in (6.23) is small enough, we can expand $\cos\theta$ and $\sin\theta$ around the resonance and approximate the functions of $\theta$ appearing in the arguments of the exponentials

$$\exp\left( [u-ct]\left\{ \left[ k_c \pm i\frac{\Gamma^2}{l} \right]\sec\theta - k_a \right\} \right) \tag{6.24}$$

and

$$\exp\left( u\left\{ \left[ k_c \pm i\frac{\Gamma^2}{l} \right]\sec\theta - k_a \right\} \right) \tag{6.25}$$

by linear functions of $\sec\theta$.

Assuming that

$$k_c \gg \frac{\Gamma_a^2}{l}, \tag{6.26}$$

the width of the resonance in (6.23) will be given by $\gamma/2ck_c$ and the resonance by $\sec\theta_c = k_a/k_c$. Then

$$\sin\theta = \sqrt{1-\left(\frac{k_c}{k_a}\right)^2} - \frac{k_c^3}{k_a^2\sqrt{k_a^2-k_c^2}}\left(\sec\theta - \frac{k_a}{k_c}\right) + (\text{higher-order terms}) \tag{6.27}$$

and

$$\cos\theta = \frac{k_c}{k_a} - \left(\frac{k_c}{k_a}\right)^2\left(\sec\theta - \frac{k_a}{k_c}\right) + (\text{higher-order terms}). \tag{6.28}$$

Then if

$$\gamma \ll \left(\frac{k_a}{k_c}\right)^2 c k_c, \tag{6.29}$$

we can substitute $\cos\theta$ and $\sin\theta$ in $u$ in exponentials (6.24) and (6.25) by

$$\cos\theta = \frac{k_c}{k_a} \tag{6.30}$$

and

$$\sin\theta = \sqrt{1-\left(\frac{k_c}{k_a}\right)^2}, \tag{6.31}$$

the integrals over $\theta$ involving the factors (6.23) will be of the kind

$$\int_1^\infty \frac{e^{i([k_c + i\Gamma_a^2/l]\sec\theta - k_a)v} f(\sec\theta)}{(k_c + i\Gamma_a^2/l)\sec\theta - k_a + i\gamma/2c} d(\sec\theta) \tag{6.32}$$

for $v>0$ and

$$\int_1^\infty \frac{e^{i([k_c - i\Gamma_a^2/l]\sec\theta - k_a)v} f(\sec\theta)}{(k_c - i\Gamma_a^2/l)\sec\theta - k_a + i\gamma/2c} d(\sec\theta) \tag{6.33}$$

for $v<0$. In these integrals, $v$ does not depend on $\sec\theta$ and $f(\sec\theta)$ has no singularities (poles). Making the change of variable $\sec\theta \to \sec\theta + k_a/k_c$ in (6.32) and extending the integral to $-\infty$, we can integrate (6.32) by contour integration. We close the contour in the upper half of the complex plane because $v>0$, but then, as the integrand has no poles in the upper half of the complex plane, integral (6.32) vanishes.

Repeating the same procedure for (6.33), we find that this time the contour has to be closed in the lower half of the complex plane because $v<0$. Now if $\gamma/2c - \Gamma_a^2 k_a/lk_c$ is negative, there will be no poles in the lower half of the complex plane and the integral (6.33) will vanish as well.

So the terms in (6.12) that involve the factors (6.23) will not contribute to the result of the integral over $\theta$ of $I_1$ and therefore can be discarded when

$$\gamma < 2c\frac{\Gamma_a^2}{l}\frac{k_a}{k_c}. \tag{6.34}$$

This condition implies that the atomic resonance is *narrower* than the cavity resonance (this condition is not satisfied by present-day semiconductor gain media such as *p-n* junctions and quantum wells; nonetheless, we will explore it further).

In this case, the atomic resonance is more important than the cavity resonance in determining the frequency of emission. Then, as we will show when we integrate over $\theta$ the remaining terms in (6.12), the cavity resonance will influence the direction of emission.

So, under conditions (6.26), (6.29), and (6.34), we obtain

$$I_1 = i2\pi \frac{\Gamma_a^2 e^{(u-ct)\gamma/2c}[k_a - i\gamma/2c]^3}{([k_a - i\gamma/2c]\cos\theta - k_c)^2 l^2 + \Gamma_a^4} \Theta(ct-u)\Theta(u), \tag{6.35}$$

where $\Theta$ is the Heaviside step function. Applying the same method to $I_2$ given by Eq. (6.13), we obtain

$$I_2 = I_1 \frac{l}{\Gamma_a}\left(\left[k_a - i\frac{\gamma}{2c}\right]\cos\theta - k_c\right). \tag{6.36}$$

If we now use (6.35) and (6.36) in (6.8) and integrate over $\theta$ following the same procedure outlined above and assuming that

$$\sqrt{(x-x_a)^2+(y-y_a)^2}\sin\theta_c \ll (z-z_a)\sin\theta_c, \tag{6.37}$$

we find that the terms involving exponentials of $i(z \pm z_a)C$, where $C$ is negative, do not have poles where the contour is closed and therefore do not contribute to the total integral. Moreover, because the detuning is small, i.e.,

$$k_a - k_c \ll k_c, \tag{6.38}$$

we also find that the $x$ and $y$ components of $\mathbf{E}^+_{s,\mathrm{out}}$ are much smaller than the $z$ component and can be neglected. Then, far from the cavity where $z \gg z_a, l$, we obtain the expression for $\mathbf{E}^+_{s,\mathrm{out}}$,

$$\mathbf{E}^+_{s,\mathrm{out}}(\mathbf{r},t) = \hat{\mathbf{x}} E_0 \sigma(0) F(x,y) e^{-(\gamma/2 + i\omega_a)(t - [z/c]\cos\theta_c)} \times \sin(k_c z_a)\Theta\left(t - \frac{z}{c}\cos\theta_c\right), \tag{6.39}$$

where

$$E_0 = -\frac{\mu\hbar k_a^3}{2\pi\varepsilon_0\Gamma_a} \tag{6.40}$$

and $F$ is the integral over $\phi$ that is still to be done

$$F(x,y) = \frac{1}{2\pi}\int_0^{2\pi} d\phi\, \exp(i[\{x-x_a\}\cos\phi + \{y-y_a\}\sin\phi]k_a\sin\theta_c). \tag{6.41}$$

Now this integral can be recognized as the Bessel function $J_0$ [65,66], i.e.,

$$F(x,y) = J_0(\sqrt{[x-x_a]^2+[y-y_a]^2}\, k_a \sin\theta_c). \tag{6.42}$$

From Eqs. (6.39) and (6.40), we notice that $\mathbf{E}^+_{s,\mathrm{out}}$ is proportional to the transmissivity of the microcavity, as expected, and depends on the mode distribution inside the microcavity, $\sin k_c z_a$, vanishing when the atom is at a node, i.e., on the surface of any of the mirrors. However, the most interesting feature of $\mathbf{E}^+_{s,\mathrm{out}}$ is that it describes a nondiffracting Bessel beam.

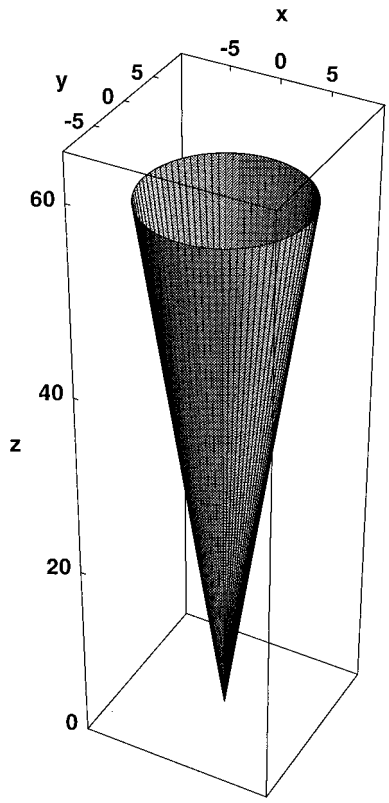


FIG. 13. Variance of the $x$ component of the electric field at the center of the cavity plotted for each mode of frequency $\omega_a = (1+\Delta)ck_c$. The fact that this surface is a cone, whose walls form an angle $\theta_c = \arccos[1/(1+\Delta)]$ with the $z$ axis, shows that emission is more likely to occur in a direction forming an angle $\theta_c$ with the $z$ axis. Such spatial frequency distribution, where the transverse component of the wave vector traces a ring, is characteristic of nondiffracting Bessel beams. The length over which the beam is essentially nondiffracting is governed by the thickness of the cone, which is determined by the finesse of the cavity. This figure is plotted for $\Delta = 0.01$ and $\Lambda_c^{-2} = 0.004$, in units of $\hbar c k_c/4\pi^3\varepsilon_0$.

Nondiffracting Bessel beams were introduced by Durnin [27], who showed that there are beam-type solutions of the wave equation for free space that do not suffer transverse spreading as they propagate. Durnin called these solutions Bessel beams because the dependence of the electric field on the transverse radial coordinate is given by a Bessel function. In a subsequent paper, Durnin *et al.* [67] reported on an experimental realization of a Bessel beam employing a thin circular slit (an annulus) located in the focal plane of a lens. When the circular slit was illuminated by collimated monochromatic light, each point within the slit acted as a point source that the lens transformed into a plane wave. The superposition of these plane waves yields the Bessel beam. Over the years, there have been many alternative proposals on how to generate Bessel beams: Herman and Wiggins [68] have shown that the beam produced by a conical lens is virtually identical to a $J_0$ beam near the optical axis. In addition, they suggested the use of spherical lenses having

spherical aberration as a method of producing Bessel $J_0$-type beams. Holographic methods have also been suggested [69–71]. Indebetouw [72] proposed the use of a Fabry-Pérot étalon to generate a Bessel beam. Some methods for producing Bessel beams had been proposed even before Durnin showed that Bessel beams do not diffract. Fujiwara [73] reported $J_0$ beams produced by using a point source and a small-angle reflecting cone. Recently, azimuthal Bessel-Gauss beam production in a concentric-circle grating surface-emitting semiconductor laser was reported [74,75].

Our result can be understood if we recall that a Bessel beam is a beam whose spatial frequency distribution forms a ring [72]. Now, the high finesse microcavity forces the emitted light to have exactly this distribution because it constrains the component of the wave vector perpendicular to the cavity mirror to assume the value $k_c$, so that every wave vector of the emitted light has to form an angle $\theta_c$ with the $z$ axis defining a ring. This is shown in Fig. 2, where we plot the variance of the $x$ component of the electric field at the center of the microcavity for each mode of frequency $\omega_a = ck_a$. The larger the variance of a given mode, the more likely it is that the atom will emit in that mode. In Fig. 13 we have plotted, in the way described in Sec. V, the variance of the $x$ component of the electric field for each mode resonant with the atomic transition. So the variance of a mode corresponding to emission in a particular direction is given by the length of the vector that points in that direction and goes from the origin to the surface. From this plot, it is clear that emission is more likely to happen in a cone of angle $\theta_c$, confirming our previous discussion. In the case examined by Indebetouw [72], because of the large dimensions of such a Fabry-Pérot étalon as compared to optical wavelengths, the wavelength of the light source is many Fabry-Pérot resonances away from the fundamental mode of the Fabry-Pérot étalon (in fact, the source of light is even placed outside the Fabry-Pérot étalon) and it is necessary to use some extra device, such as lenses, in order to select the right mode.

## VII. SUMMARY

In this paper we have showed that cavity QED in a planar microcavity can modify the angular distribution of atomic spontaneous emission in such a way that nondiffracting Bessel beams may be generated. Of course a classical dipole in such a geometry would also generate a nondiffracting Bessel beam as this is a consequence solely of the cavity mode structure and detuning. However, as we are interested in the possibility of investigating, in the future, the quantum noise in the light from these sources, we have adopted a fundamental quantum viewpoint of the emission. The degree to which the beam is actually nondiffracting (i.e., the propagation distance over which diffraction is eliminated) is governed by the finesse of the microcavity. We have concentrated here on atomic spontaneous-emission from a single isolated two-level atom in a high-finesse microcavity. It has not escaped our attention that a quantum-dot semiconductor source, provided it is suitably confined to a region small enough, may well generate such a nondiffracting output from such a cavity and eliminate the diffractive spread, which could otherwise plague these devices. The length over which the beam is actually nondiffractive is governed by the cavity length and the finesse.

## ACKNOWLEDGMENTS

This work was supported in part by the European Community, the United Kingdom Engineering and Physical Sciences Research Council, and by CAPES (Fundação Coordenação de Aperfeiçoamento de Pessoal de Nível Superior). The authors would also like to thank S. Chavez-Cerda, M. A. Rippin, and E. S. Guerra for discussions.

[1] P. Filipowicz, P. Meystre, G. Rempe, and H. Walther, Opt. Acta **32**, 1105 (1985).
[2] S. Haroche, in *1990 Les Houches Lectures, Session LIII: Fundamental Systems in Quantum Optics*, edited by J. Dalibard, J.-M. Raimand, and J. Zinn-Justin (North-Holland, Amsterdam, 1992).
[3] S. Haroche and D. Kleppner, Phys. Today **1** (1), 24 (1989).
[4] F. De Martini, G. Innocenti, G. R. Jacobovitz, and P. Mataloni, Phys. Rev. Lett. **59**, 2955 (1987).
[5] W. Jhe, A. Anderson, E. A. Hinds, D. Meschede, L. Moi, and S. Haroche, Phys. Rev. Lett. **58**, 666 (1987).
[6] D. J. Heinzen, J. J. Childs, J. E. Thomas, and M. S. Feld, Phys. Rev. Lett. **58**, 1320 (1987).
[7] K. An, J. Childs, R. R. Dasari, and M. S. Feld, Phys. Rev. Lett. **73**, 3375 (1994).
[8] S. John, Phys. Rev. Lett. **53**, 2169 (1984).
[9] E. Yablonovitch, Phys. Rev. Lett. **58**, 2059 (1987).
[10] N. W. Ashcroft and N. D. Mermin, *Solid State Physics* (Holt, Rinehart and Winston, New York, 1976).
[11] K. M. Ho, C. T. Chan, and C. M. Soukoulis, Phys. Rev. Lett. **65**, 3152 (1990).
[12] J. W. Haus, J. Mod. Phys. **41**, 195 (1994).
[13] E. Yablonovitch, J. Mod. Opt. **41**, 173 (1994).
[14] T. Sakaguchi, F. Koyama, and K. Iga, Electron. Lett. **24**, 928 (1988).
[15] M. Oshikiri, H. Kawasaki, F. Koyama, and K. Iga, IEEE Photon. Technol. Lett. **1**, 11 (1989).
[16] M. Born and E. Wolf, *Principles of Optics* (Pergamon, New York, 1970).
[17] J. L. Jewell, J. P. Harbison, A. Scherer, Y. H. Lee, and L. T. Florez, IEEE J. Quantum Electron. **27**, 1332 (1991).
[18] H. Soda, K. Iga, C. Kitahara, and Y. Suematsu, Jpn. J. Appl. Phys. **18**, 2329 (1979).
[19] O. Svelto, *Principles of Lasers* (Plenum, New York, 1989).
[20] A. Ibariki, K. Kawashima, K. Furusawa, T. Ishikawa, T. Yamagushi, and T. Nina, Jpn. J. Appl. Phys. **28**, L667 (1989).
[21] F. De Martini and G. Innocenti, in *Quantum Optics IV*, edited by J. D. Harvey and D. F. Walls (Springer-Verlag, Heidelberg, 1986).
[22] F. De Martini and G. R. Jacobovitz, Phys. Rev. Lett. **60**, 1711 (1988).
[23] Y. Yamamoto, S. Machida, K. Igeta, and G. Björk, in *Coherence, Amplification, and Quantum Effects in Semiconductor*

*Lasers*, edited by Y. Yamamoto (Wiley, New York, 1991), p. 561.
[24] R. P. Stanley, R. Houdré, U. Oesterle, M. Ilegems, and C. Weisbuch, Phys. Rev. A **48**, 2246 (1993).
[25] G. Lindblad, Commun. Math. Phys. **48**, 119 (1976).
[26] E. M. Purcell, Phys. Rev. **69**, 681 (1946).
[27] J. Durnin, J. Opt. Soc. Am. A **4**, 651 (1987).
[28] S. M. Dutra and P. L. Knight, Opt. Commun. **117**, 256 (1995).
[29] M. B. Spencer and W. E. Lamb, Jr., Phys. Rev. A **5**, 884 (1972).
[30] R. Lang, M. O. Scully, and W. E. Lamb, Jr., Phys. Rev. A **7**, 1788 (1973).
[31] B. Baseia and H. M. Nussenzveig, Opt. Acta **31**, 39 (1984).
[32] I. Guedes, J. C. Penaforte, and B. Baseia, Phys. Rev. A **40**, 2463 (1989).
[33] J. C. Penaforte and B. Baseia, Phys. Rev. A **30**, 1401 (1984).
[34] K. Ujihara, Phys. Rev. A **12**, 148 (1975); Jpn. J. Appl. Phys. **15**, 1529 (1976); Phys. Rev. A **16**, 652 (1977); **18**, 659 (1978); **20**, 1096 (1979).
[35] C. W. Gardiner and C. M. Savage, Opt. Commun. **50**, 173 (1984).
[36] M. Ley and R. Loudon, J. Mod. Opt. **34**, 227 (1987).
[37] K. Ujihara and X.-P. Feng, Phys. Rev. A **41**, 2668 (1990).
[38] J. Gea-Banacloche, N. Lu, L. M. Pedrotti, S. Prasad, M. O. Scully, and K. Wódkiewicz, Phys. Rev. A **41**, 369 (1990); **41**, 381 (1990).
[39] S. M. Barnett and P. M. Radmore, Opt. Commun. **68**, 364 (1988).
[40] L. Knöll, W. Vogel, and D.-G. Welsch, J. Mod. Opt. **38**, 55 (1991); Phys. Rev. A **43**, 543 (1991).
[41] J. J. Hopfield, Phys. Rev. **112**, 1555 (1958).
[42] M. Hillery and L. D. Mlodinow, Phys. Rev. A **30**, 1860 (1984).
[43] L. Knöll, W. Vogel, and D.-G. Welsch, Phys. Rev. A **36**, 3803 (1987).
[44] R. J. Glauber and M. Lewenstein, Phys. Rev. A **43**, 467 (1991).
[45] B. Huttner and S. M. Barnett, Phys. Rev. A **46**, 4306 (1992).
[46] J. D. Jackson, *Classical Electrodynamics* (Wiley, New York, 1975).
[47] A. G. Fox and T. Li, Bell Syst. Tech. J. **40**, 453 (1961).
[48] C. Cohen-Tannoudji, J. Dupont-Roc, and G. Grynberg, *Photons and Atoms: Introduction to Quantum Electrodynamics* (Wiley, New York, 1989).
[49] F. De Martini, M. Marrocco, P. Mataloni, L. Crescentini, and R. Loudon, Phys. Rev. A **43**, 2480 (1991).
[50] E. A. Hinds, Adv. At. Mol. Opt. Phys. **28**, 237 (1991).
[51] L. Allen and J. H. Eberly, *Optical Resonance and Two-Level Atoms* (Dover, New York, 1987).
[52] H. Morawitz, Phys. Rev. **187**, 1792 (1969).
[53] F. T. Arecchi and E. Courtens, Phys. Rev. A **2**, 1730 (1970).
[54] P. W. Milonni, Opt. Commun. **8**, 60 (1973).
[55] P. W. Milonni and P. L. Knight, Opt. Commun. **9**, 119 (1973).
[56] J. P. Dowling, M. O. Scully, and F. De Martini, Opt. Commun. **82**, 415 (1991); J. P. Dowling, in *Measurements in Optics*, edited by D. F. Walls (Plenum, New York, 1992).
[57] R. H. Dicke, Phys. Rev. **93**, 99 (1954).
[58] H. Kuhn, J. Chem. Phys. **53**, 101 (1970).
[59] K. H. Drexhage, Habilitation thesis, University of Marburg, Germany, 1966 (unpublished); in *Progress in Optics XII*, edited by E. Wolf (North-Holland, Amsterdam, 1974), p. 163.
[60] J. Dalibard, J. Dupont-Roc, and C. Cohen-Tannoudji, J. Phys. (Paris) **43**, 1617 (1982).
[61] P. W. Milonni, Phys. Scr. **T21**, 102 (1988).
[62] H. Yokoyama and S. D. Brorson, J. Appl. Phys. **66**, 4801 (1989).
[63] G. Björk and Y. Yamamoto, IEEE J. Quantum Electron. **27**, 2386 (1991).
[64] This is true for atoms, but excitons can couple to a single longitudinal mode $\mathbf{k}=k_{z,n}\hat{\mathbf{z}}$ of a planar microcavity, ignoring the continuum of lateral modes corresponding to continuous values of the projection of the wave vector $\mathbf{k}$ on the $x$-$y$ plane. In fact, vacuum Rabi splitting has been observed for excitons in microcavities; see C. Weisbuch, M. Nishioka, A. Ishikawa, and Y. Arakawa, Phys. Rev. Lett. **69**, 3314 (1992).
[65] A. Erdélyi, W. Magnus, F. Oberhettinger, and F. G. Tricomi, *Higher Transcendental Functions* (McGraw-Hill, New York, 1953).
[66] J. Mathews and R. L. Walker, *Mathematical Methods of Physics* (Addison-Wesley, Menlo Park, CA, 1973).
[67] J. Durnin, J. J. Miceli, Jr., and J. H. Eberly, Phys. Rev. Lett. **58**, 1499 (1987); see also J. Durnim, J. J. Miceli, and J. H. Eberly, *ibid.* **66**, 837 (1991); T. Wulle and S. Herminghaus, *ibid.* **71**, 209 (1993).
[68] R. M. Herman and T. A. Wiggins, J. Opt. Soc. Am. A **8**, 932 (1991).
[69] J. Turunen, A. Vasara, and A. T. Friberg, Appl. Opt. **27**, 3959 (1988).
[70] A. Vasara, J. Turunen, and A. T. Friberg, J. Opt. Soc. Am. A **6**, 1748 (1989).
[71] N. Davidson, A. A. Friesem, and E. Hasman, Opt. Commun. **88**, 326 (1992).
[72] G. Indebetouw, J. Opt. Soc. Am. A **6**, 150 (1989).
[73] S. Fujiwara, J. Opt. Soc. Am. **52**, 287 (1962).
[74] T. Erdogan, O. King, G. W. Wicks, D. G. Hall, H. Anderson, and M. J. Rooks, Appl. Phys. Lett. **60**, 1921 (1992).
[75] R. H. Jordan and D. G. Hall, Opt. Lett. **19**, 427 (1994).